Received: 9 January 2020 | Accepted: 7 August 2020

DOI: 10.1111/1365-2745.13493

Check for updates

Journal of Ecology | BRITISH ECOLOGICAL SOCIETY

RESEARCH ARTICLE

Bridging ecology and physics: Australian fairy circles regenerate following model assumptions on ecohydrological feedbacks

Stephan Getzin[1,2] | Todd E. Erickson[3,4] | Hezi Yizhaq[5] | Miriam Muñoz-Rojas[3,4,6] | Andreas Huth[2] | Kerstin Wiegand[1]

[1]Department of Ecosystem Modelling, University of Goettingen, Goettingen, Germany; [2]Department of Ecological Modelling, Helmholtz Centre for Environmental Research – UFZ, Leipzig, Germany; [3]School of Biological Sciences, The University of Western Australia, Crawley, WA, Australia; [4]Department of Biodiversity, Conservation and Attractions, Kings Park Science, Perth, WA, Australia; [5]Department of Solar Energy and Environmental Physics, Ben-Gurion University of the Negev, Sede Boqer, Israel and [6]School of Biological, Earth and Environmental Sciences, Centre for Ecosystem Science, UNSW Sydney, Sydney, NSW, Australia

Correspondence
Stephan Getzin
Email: stephan.getzin@uni-goettingen.de

Funding information
German Research Foundation - DFG, Grant/Award Number: 323093723

Handling Editor: Susan Schwinning

Abstract

1. So-called fairy circles (FCs) comprise a spatially periodic gap pattern in arid grasslands of Namibia and north-west Western Australia. This pattern has been explained with scale-dependent ecohydrological feedbacks and the reaction-diffusion, or Turing mechanism, used in process-based models that are rooted in physics and pattern-formation theory. However, a detailed ecological test of the validity of the modelled processes is still lacking.
2. Here, we test in a spinifex-grassland ecosystem of Western Australia the presence of spatial feedbacks at multiple scales. Drone-based multispectral analysis and spatially explicit statistics were used to test if grass vitality within five 1-ha plots depends on the pattern of FCs that are thought to be a critical extra source of water for the surrounding matrix vegetation. We then examined if high- and low-vitality grasses show scale-dependent feedbacks being indicative of facilitation or competition. Additionally, we assessed facilitation of grass plants for different successional stages after fire at fine scales in 1-m^2 quadrats. Finally, we placed soil moisture sensors under bare soil inside the FC gap and under plants at increasing distances from the FC to test if there is evidence for the 'infiltration feedback' as used in theoretical modelling.
3. We found that high-vitality grasses were systematically more strongly associated with FCs than low-vitality grasses. High-vitality grasses also had highly aggregated patterns at short scales being evidence of positive feedbacks while negative feedbacks occurred at larger scales. Within 1-m^2 quadrats, grass cover and mutual facilitation of plants was greater near the FC edge than further away in the matrix. Soil moisture after rainfall was lowest inside the FC with its weathered surface

This is an open access article under the terms of the Creative Commons Attribution License, which permits use, distribution and reproduction in any medium, provided the original work is properly cited.
© 2020 The Authors. *Journal of Ecology* published by John Wiley & Sons Ltd on behalf of British Ecological Society

crust but highest under grass at the gap edge, and then declined towards the matrix, which confirms the infiltration feedback.

4. *Synthesis*. The study shows that FCs are a critical extra source of water for the dryland vegetation, as predicted by theoretical modelling. The grasses act as 'ecosystem engineers' that modify their hostile, abiotic environment, leading to vegetation self-organization. Overall, our ecological findings highlight the validity of the scale-dependent feedbacks that are central to explain this emergent grassland pattern via the reaction-diffusion or Turing-instability mechanism.

KEYWORDS

ecosystem engineer, Normalized Difference Vegetation Index, reaction-diffusion mechanism, scale-dependent feedback, spatial periodicity, Turing dynamics, unmanned aerial vehicle, vegetation self-organization

1 | INTRODUCTION

Spatially periodic plant patterns in drylands such as vegetation spots at the transition to bare-soil desert, stripes of trees and grasses or vegetation gaps have attracted the attention of scientists for many decades. The fascination about such highly ordered distributions was, and is, induced by inspecting aerial imagery because the invariable spatial periodicity of such regular patterns is only visible from a bird's-eye view. Examples include tree bands such as 'tiger bush' (Boaler & Hodge, 1962; Lefever & Lejeune, 1997), banded grass patterns (Worrall, 1959) and shrubland gaps (Barbier, Couteron, Lefever, Deblauwe, & Lejeune, 2008) in arid Africa, tree stripes (Dunkerley, 2002; Saco, Willgoose, & Hancock, 2007) and banded grass (Dunkerley & Brown, 1999) in Australia or many other gap, stripe, labyrinth and spot patterns from water-limited environments around the globe (Deblauwe, Barbier, Couteron, Lejeune, & Bogaert, 2008). These well-known vegetation patterns are thought to emerge primarily due to short-range positive ecohydrological biomass-water feedbacks and resultant long-range water depletion, and the forming morphologies follow specific rules of pattern-formation theory (Borgogno, D'Odorico, Laio, & Ridolfi, 2009; Couteron & Lejeune, 2001; Deblauwe, Couteron, Lejeune, Bogaert, & Barbier, 2011; Meron, 2012, 2016; Meron et al., 2019; Meron, Gilad, von Hardenberg, Shachak, & Zarmi, 2004).

One of the most striking vegetation patterns are the so-called 'fairy circles' which occur in the arid grasslands of Namibia (van Rooyen, Theron, van Rooyen, Jankowitz, & Matthews, 2004) and east of Newman in north-west Western Australia (Getzin et al., 2016). In these largely homogeneous sandy or clayish habitats, where only one or two grass species predominate, the fairy circles have diameters of typically 4–10 m and they have an identical spatial signature. This signature is characterized by each fairy circle having on average six nearest neighbours that are located at approximately the same distance from the focal circle, leading to a hexagonal grid. The fairy circles are thus spatially periodic and constitute probably the most regularly distributed vegetation gaps that are currently known from arid environments (Getzin, Yizhaq, Cramer, & Tschinkel, 2019; Getzin, Yizhaq, Munoz-Rojas, Wiegand, & Erickson, 2019). It is obvious that such exceptionally ordered patterns can only result from strong interactive processes, because in the absence of interaction, the probability of creating order in a noisy environment is very unlikely (Saha & Galic, 2018).

Fairy circles (FCs) are subject to an ongoing controversy about their origin (Sahagian, 2017). More recent theories have focused on vegetation self-organization and argued that FCs are an emergent vegetation phenomenon that reflects a population-level response to aridity stress where ecohydrological biomass-water feedbacks lead to strictly geometric patterns (Cramer & Barger, 2013; Cramer, Barger, & Tschinkel, 2017; Getzin et al., 2015a,b; 2016; Getzin, Yizhaq, Cramer, et al., 2019; Ravi, Wang, Kaseke, Buynevich, & Marais, 2017; Zelnik, Meron, & Bel, 2015). The periodically ordered pattern is thus an expression that there is not enough water to sustain uniform vegetation coverage at the landscape scale and the distinct, so-called 'wavelength' of the gap pattern reflects the spatial scale at which water is most limiting to the plants (Meron, 2016).

One point of criticism, however, is that the support of this hypothesis was mainly rooted in physics and mathematical modelling of pattern formation while there are currently too little field-based studies to verify the validity of such models (Vlieghe & Picker, 2019). Indeed, there is a strong imbalance between the theoretical vegetation models, their a priori assumptions and the scarcity of empirical proof that the modelled processes are correct from an ecological point of view. This imbalance can be attributed to the fact that the recognition of periodically ordered vegetation in drylands has primarily drawn the interest of physicists to replicate the observed patterns via partial-differential equation modelling (Klausmeier, 1999; Lefever & Lejeune, 1997; Rietkerk et al., 2002; von Hardenberg, Meron, Shachak, & Zarmi, 2001; Yizhaq & Bel, 2016). Very few such studies in arid environments, however, have empirically linked measured processes and ecological properties in the field with the theoretical modelling of the assumed ecohydrological feedbacks and resultant vegetation self-organization.

These include studies of vegetation gaps in African shrublands (Barbier et al., 2008) or ring formation in Israelian desert plants (Yizhaq, Stavi, Swet, Zaady, & Katra, 2019). With a similar empirical approach, other studies from moister climates include, for example, peatlands in Siberia (Eppinga et al., 2008; Eppinga, de Ruiter, Wassen, & Rietkerk, 2009).

With regard to the FCs, the major empirical support for the vegetation models currently comes from analyses of higher-level components and so-called coarse-graining, hence from aggregating finer-scale processes or patterns to larger-scale summaries (Newman, Kennedy, Falk, & McKenzie, 2019). For example, the modelled FC patterns have been statistically matched with FC snap-shot patterns in aerial imagery (Getzin et al., 2015a, 2016) or the rainfall-dependent appearance and disappearance of FCs, as observed in satellite images, has been well replicated with dynamic modelling (Zelnik et al., 2015). In context with pattern-oriented modelling (Grimm et al., 2005; Wiegand, Saltz, Ward, & Levin, 2008), these vegetation models that are based on theoretically assumed processes of plant competition for soil water have, in principle, the ability to replicate the coarse-grained FC spatial structure. Similar successful matching of modelled and real-world patterns has also been demonstrated for completely different systems such as the Everglades in Florida (Acharya, Kaplan, Casey, Cohen, & Jawitz, 2015) or Mediterranean seagrass meadows (Ruiz-Reynés et al., 2017).

This successful matching, however, is not a verification that the modelled processes and mechanisms of plant self-organization are indeed right and happening in the real world to cause the observed patterns (Borgogno et al., 2009). Within a framework of pattern-process inference, these coarse-graining methods are mainly useful to identify unlikely processes for the cause of the pattern and to narrow down the most plausible working hypotheses (Getzin, Yizhaq, Cramer, et al., 2019; McIntire & Fajardo, 2009; Schurr, Bossdorf, Milton, & Schumacher, 2004). Consequently, if the extensive achievements of the mathematical process-based models are to find greater acceptance in ecology, then it is necessary not only to reconstruct the higher-level structures but also to demonstrate true evidence of the validity of the modelled lower-level processes assumed a priori. This can be achieved with more fine-grained and detailed ecological analyses in the field, including experimental testing (Tschinkel, 2015), plant- and soil-related ecohydrological measurements (Cramer et al., 2017; Getzin et al., 2016; Ravi et al., 2017) and high-resolution vegetation mapping employing modern drones (Getzin, Wiegand, & Schoening, 2012; Getzin, Yizhaq, Munoz-Rojas, et al., 2019).

Process-based FC vegetation models use nonlinear partial-differential equations to reconstruct the periodic FC ordering via so-called Turing-like instabilities, also called Turing mechanisms, and principles of pattern-formation theory (Borgogno et al., 2009; Meron, 2012, 2015; Turing, 1952). This Turing mechanism is also known as reaction-diffusion mechanism or activator-inhibitor principle, and a key to forming spatially periodic Turing patterns is the presence of positive and negative feedback interaction at different spatial scales (Figure 1a; Rietkerk & van de Koppel, 2008). In context with modelling self-organized vegetation patterns in drylands, ecohydrological feedback loops with positive short-range plant interaction (facilitation) but negative long-range inhibition (competition) are central to explain the periodically ordered FCs (Figure S1; Getzin et al., 2016; Meron, 2018; Tlidi, Lefever, & Vladimirov, 2008). Such models generally predict two uniform stable states—uniform vegetation under high precipitation and bare-soil desert at lowest rainfall. Between these two stable states, periodically ordered states such as FCs, vegetation spots, stripes and labyrinths can form and the various proportions of bare soil are an expression that there is not enough water to sustain a continuous or uniform vegetation layer (Figure 1b–d; Meron, 2018). Fundamental to these processes is that various modes of water transport are capable of inducing pattern-forming feedbacks in water-limited vegetation (Meron, 2012, 2016) so that resource concentration leads to self-organized patchiness and a local aggregation of biomass (Rietkerk, Dekker, de Ruiter, & van de Koppel, 2004).

For Namibian FCs, which form primarily on deep aeolian sands, the mode of soil-water diffusion towards spatially confined grass roots has been identified as the dominant feedback mechanism to model the FCs (Zelnik et al., 2015). For Australian FCs, which form as hard weathered clay crusts, overland-water flow and an 'infiltration feedback' have been successfully used to model the process of local water uptake by the spinifex grasses of the genus *Triodia* (Figure 1e, Figure S1; Getzin et al., 2016). Here, the a priori assumption is that the roots of the *Triodia* plants induce an infiltration contrast and thereby trigger the positive short-range feedback loop where more vital and larger plants gain more water and thus have a disproportionally greater benefit than weaker neighbouring plants (Figure 1f). Irrespective of the differences between these proposed feedback mechanisms in Namibia and Australia, it is assumed that the emergent FCs contribute a critical extra source of water for the surrounding matrix grasses that grow between the FCs and that the most vital grasses should therefore grow around the FC perimeters. By forming periodic vegetation-gap patterns, the grasses benefit from the additional water resource provided by the FCs, and thereby keep the ecosystem functional at precipitation values lower than those required for uniform vegetation (Meron, 2018). In this way, the grasses act as 'ecosystem engineers' because their cooperative action modifies the abiotic environment, they redistribute resources and they facilitate the growth of their own species in their canopy neighbourhood (Borgogno et al., 2009; Gilad, von Hardenberg, Provenzale, Shachak, & Meron, 2004).

Despite the intriguing periodic vegetation patterns in global drylands, there are still only very few studies where field-based data have been directly linked to the theoretical modelling of reaction-diffusion processes and the a priori assumed feedback mechanisms (Barbier et al., 2008; Dunkerley, 2018; Yizhaq et al., 2019). This current lack of bridging between ecology and physics is no surprise given that most of the papers dealing with such periodic dryland vegetation are based on modelling, but there is a gap between the relative mathematical simplicity of the models and

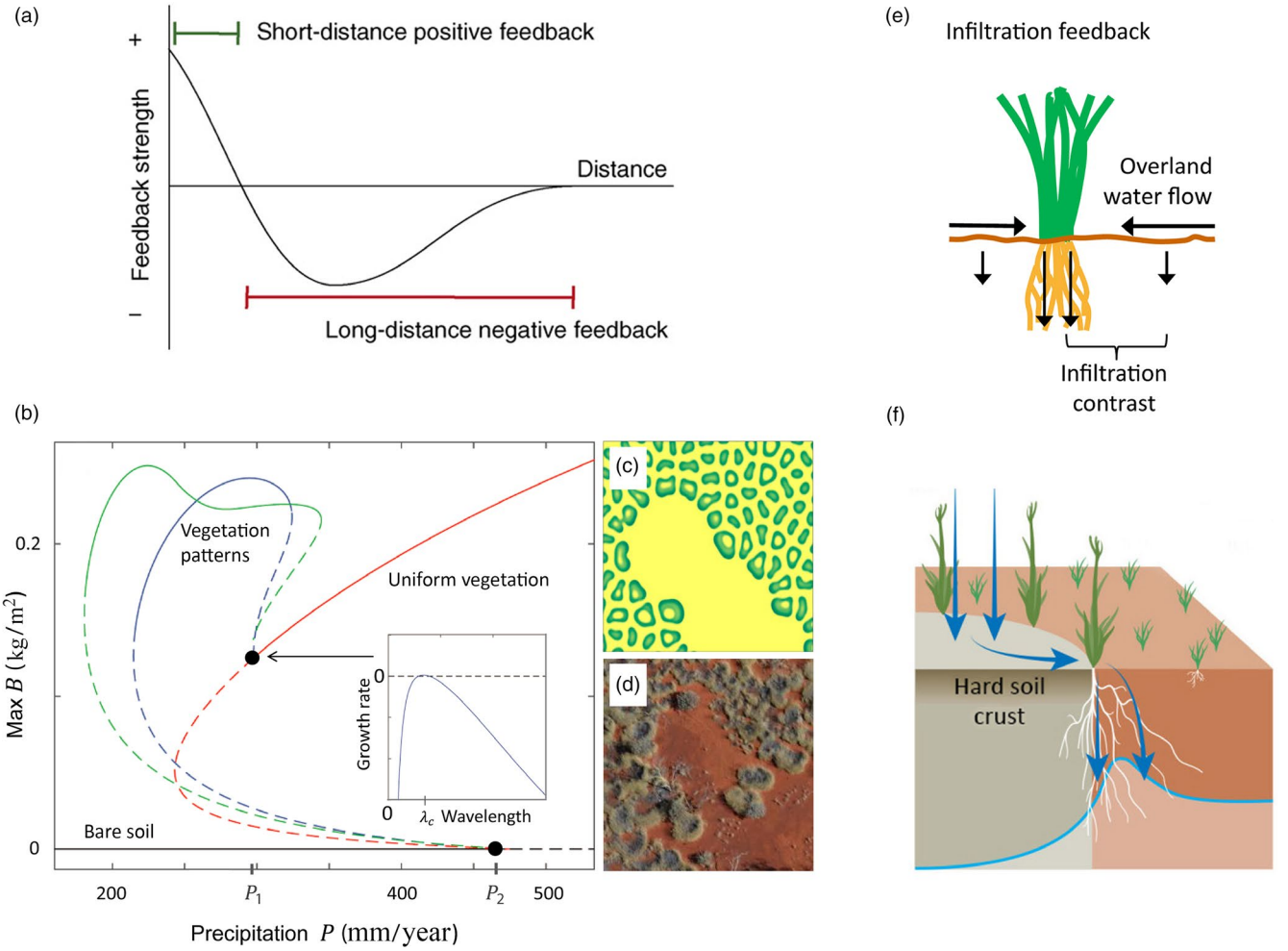

FIGURE 1 Modelling the fairy circles of Australia based on principles of pattern-formation theory. A short-distance positive feedback and a long-distance negative feedback is central to generate a Turing pattern (a, after Rietkerk & van de Koppel, 2008). A bifurcation diagram (b), used for modelling the Australian FCs and visual agreement of modelled (c) and real-world (d) patterns of *Triodia* plants. The black and red solid lines in the diagram (b) show stable bare soil and uniform vegetation, respectively, and the blue and green lines show two examples of periodic vegetation patterns that the system can take on (details in Getzin et al., 2016). The model is based on a specific pattern-forming feedback, which is overland-water flow due to infiltration contrast (e). This modelled mechanism leads to lowest soil moisture inside the FC but highest soil moisture and the most vigorous plant growth at the FC edge, which then declines towards the matrix (f, after Palmer, 2016; see also Figure S1)

the complexity of the real world (Kondo & Miura, 2010). Moreover, while the reaction-diffusion mechanism is now widely accepted for Turing patterns at the subcellular or cellular levels (e.g. pigmentation in zebrafish), for the organismal level such as dryland vegetation, empirical evidence is still rare (Saha & Galic, 2018). So far, there is mostly no conclusive experimental evidence suggesting that the organized spatial configurations of vegetation observed in nature do emerge from Turing-like dynamics (Borgogno et al., 2009).

Besides the aforementioned field studies, empirical support for the validity of Turing dynamics does partially also exist with regard to fairy circles. For example, in Namibia it has been demonstrated that the deep aeolian sands form a hydraulically connected edaphic environment where water is highly mobile and may laterally flow more than seven metres within a short time (Cramer et al., 2017). These scales of horizontal water movement equal biomass gradients where the strongest and most vital grasses can be found around the FCs while less vital grasses grow metres away from the FCs. The high mobility of water in deep aeolian sand therefore justifies using fast soil-water diffusion as the specific feedback mechanism to model the Namibian FCs (Zelnik et al., 2015).

For the Australian FCs, fieldwork has demonstrated that water infiltration in unvegetated soil inside the FCs is significantly lower than in soils between the surrounding matrix vegetation. Preliminary experimental testing has also shown that despite the flatness of the landscape, excess surface water moves from the FCs towards the matrix due to strongly reduced infiltration within the FC, which resulted in using the infiltration feedback as the specific mechanism to model the Australian FCs (Figure 1e; Getzin et al., 2016). Based on more than 150 soil excavations it has also been demonstrated that these FCs have no causal link to termite activity but that their high clay contents and soil compaction results from mechanical abiotic

weathering in this climatically harsh environment (Getzin, Yizhaq, Munoz-Rojas, et al., 2019). These findings are so far in support of the modelled infiltration contrast, but they do not yet constitute a detailed ecological test of the validity of the model assumptions and associated feedback mechanisms. Indeed, identification and verification of the specific dynamics of the reaction-diffusion system is critical to showing the applicability of the Turing mechanism to the formation of a given pattern (Kondo & Miura, 2010). Therefore, we need to test specific model assumptions such as (a) the landscape-scale function of the FC pattern as a critical extra source of water for the matrix vegetation, (b) the scale-dependent feedbacks of vegetation interaction and (c) the existence of the infiltration feedback. For this reason, we have undertaken a holistic ecological study in north-west Western Australia to test if the a priori assumed processes from physics and the modelled ecohydrological feedback mechanisms can be verified in the real world. We focused here only on the Australian FCs due to the considerable labour effort that is necessary to test those processes and secondary model predictions over longer time scales and large spatial scales. Here we tested the following hypotheses.

Hypothesis 1 *According to the reaction-diffusion mechanism, the formation of a spatially structured mode, i.e. the periodically ordered FC pattern across the landscape, is not a random event but inherently linked to the demography and ecohydrological feedbacks of the grass population. Grasses of high vitality should show a stronger spatial association with the FCs than low-vitality grasses because the FCs are assumed to have a landscape-scale function as a critical extra source of water for the vegetation. We tested this model assumption by using high-resolution, multispectral drone imagery and spatially explicit statistics, as well as classic landscape metrics.*

Hypothesis 2 *If the FCs result from positive and negative feedback interactions of the grasses, then high-vitality grasses which primarily exert positive feedbacks and facilitation should principally have strongly clustered distributions at short scales and increasingly merge at the FC gap edge to increase their benefit from higher water availability. In contrast, low-vitality grasses which suffer from a lack of water and negative feedbacks, should not have clustered but regular to random distributions at scales slightly larger than the positive feedback. This is because a poor water availability should not support a cooperative patch formation of clumped grasses but only the survival of scattered or segregated individuals that are more widely spaced. This model assumption is also tested using drone imagery and spatial statistics, as well as fine-scale mapping of post-fire grass recovery within sample quadrats placed at edge and matrix locations around FCs.*

Hypothesis 3 *If the pattern-forming processes based on the modelled infiltration feedback are verifiable, there should be a high infiltration contrast between the bare soil of the FCs and under bordering plants at the FC periphery where root conduits aid in increased water infiltration. Most water should infiltrate under alive plants that directly border on the FC edge, less water should infiltrate further away in the matrix and least water in the interior of the hardened FC. This fundamental model assumption about the feedback mechanism was tested with the installation of a fully equipped weather station containing soil moisture and temperature sensors.*

2 | MATERIALS AND METHODS

2.1 | Study area

The Australian FCs can be found in a small area near the mining town of Newman in the Pilbara region of north-west Western Australia. They exist only within a radius of 10 km east to south of Ophthalmia Dam, which is fed by the Fortescue River upper catchment (Getzin et al., 2016; Getzin, Yizhaq, Munoz-Rojas, et al., 2019). This landscape is very flat and mono-specifically dominated by the spinifex grass *Triodia basedowii* E. Pritz. Soils on the flat plains are sandy, comprising Red Kandosols, Red Ferrosols and Leptic Rudosols (Isbell, 2002). The climate is arid with about 330 mm mean annual precipitation (MAP) over the period 1972–2018, and 3,200–3,400 mm annual evaporation, representing an aridity index of *c*. 0.1. During the summer tropical cyclone season from November to April, exceptionally strong rainfall events may occur with rainfall exceeding 50 mm on one single day (Australian Government Bureau of Meteorology, 2018). Air temperatures during the summer cyclone season can be very high with daily maxima exceeding 45°C. Soil surface temperatures in the upper centimetre on bare ground in FCs can reach 75°C, and mechanical weathering in these harsh conditions leads to the formation of physical clay crusts with compacted and sealed surfaces, which hamper rain infiltration and cause runoff water to flow on the surface (Getzin et al., 2016; Getzin, Yizhaq, Munoz-Rojas, et al., 2019). Recurrent natural fire events, which may be spatially patchy, burn these *Triodia* grasslands approximately every 15–30 years, thereby destroying the entire grass vegetation (Levin, Levental, & Morag, 2012; Muñoz-Rojas, Erickson, Martini, Dixon, & Merritt, 2016). *Triodia basedowii* regenerates entirely from seeds after fire (Grigg, Veneklaas, & Lambers, 2008).

2.2 | Drone survey

Between the 7th and 25th of July 2017, we undertook a drone (unmanned aerial vehicle, UAV) survey where we mapped five FC plots with a Microdrone md4-1000 quadcopter (Figure 2a,b). Their location has been described in Getzin, Yizhaq, Munoz-Rojas, et al. (2019) for four of these plots, named 'FC-L1', 'FC-L2', 'FC-C2', 'FC-1', and in Getzin et al. (2016) for the fifth plot, named 'FC-C5' (Table S1; Figure S2a). The plots FC-L1, FC-L2 and FC-C5 represent typical climax stages of long unburnt *Triodia* grasslands (i.e. >15 years since fire). These plots, however, experienced a severe fire during the year after the survey, on 6th of April 2018, which burnt the entire grass layer. The plot FC-C2 burnt in early November 2014, thus at the time

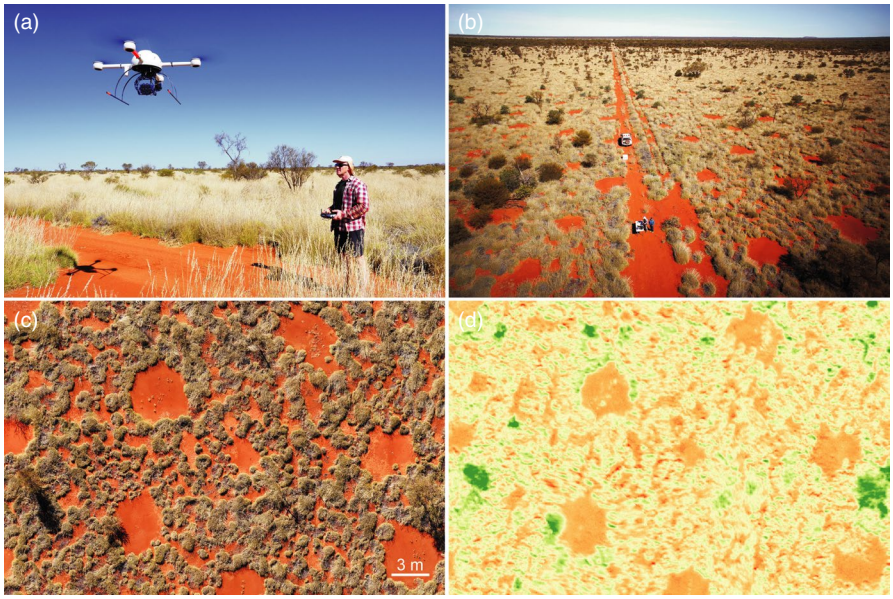

FIGURE 2 Lifting off with the Microdrone md4-1000 quadcopter and the mounted multispectral camera Tetracam Mini MCA-6 (a). View from the drone over the arid *Triodia* grassland and the plot FC-L1 in Western Australia (b). Example of a drone-acquired RGB photo with scale bar (c) and a matched NDVI image (d) of Australian FCs in plot FC-C5, mapped in 2017 with the Microdrone md4-1000. In the colour palette of image (d), darker green shows woody shrubs and trees, yellowish-green indicates vital grasses while light-yellowish shows less vital grasses. Transitions between dead lignified grasses and litter towards bare soil, classified as 'noise', are indicated by very light-yellowish to brownish colours. Mechanical clay crusts of typical bare soil are indicated as brownish to reddish colours

of the survey, the recovering vegetation was 2 years and 8 months old for plot FC-C2. Plot FC-1 burnt sometime between 2005 and 2012. According to plant size, this plot has an estimated post-fire age of about 10 years.

In order to achieve ultra-high resolution mapping of 1 cm/pixel with the 24-megapixel photo camera SONY NEX-7, plot sizes were limited to 200 m × 200 m, flying altitude was 40 m above ground, flying speed was 3 m/s and 420 RGB images were taken with 85% forward and 70% sideward overlap (Figure 2c; Figure S2b). These images were used as visual backup but were not further analysed.

The same plots were then mapped with the multispectral camera Tetracam Mini MCA-6, which has 1.3-megapixel sensors for each of the six channels with bandpass filters of 550, 670, 710, 780, 900 and 950 nanometres respectively. Unlike the photo camera with a wide-angle lens, the Tetracam has a tele lens, which required a flying altitude 100 m above ground to cover the 200 m × 200 m plots with one continuous flight. At a flying speed of 3 m/s, 250 photos were taken with 85% forward, 70% sideward overlap and a resolution of 6 cm/pixel (Figure 2d).

2.3 | Preparation of drone data

OneButton software (www.icaros.us) was used to stitch the RGB photos and the multispectral images into geo-referenced ortho-photos. The RGB photos were directly fed into the software. The multispectral images from raw Tetracam files were at first converted into multipage TIFF images with the software PixelWrench 2 and then stitched together. Using OneButton software, we calculated the Normalized Difference Vegetation Index (NDVI) with the formula NDVI = (NIR − Red)/(NIR + Red), based on the bandpass filters of 670 nm (Red) and 900 nm (NIR) respectively (Figure 2d). The obtained NDVI images were then inspected for the range of NDVI values being typical for bare soil, bare soil partly covered by dead lignified grasses and litter, low-vitality grasses, high-vitality grasses and woody vegetation such as shrubs and eucalypt trees that also occur in the FC plots. NDVI values >0.10 up to maximum values of 0.52 were classified as green leaves of shrubs and trees. Lowest NDVI values ranging from −0.37 to ≤−0.26 were identified as bare soil without litter coverage, while values ranging from −0.25 to ≤−0.16 turned out to be bare soil-litter transitions where soil was partly covered with lignified remnants of dead *Triodia* grasses. The remaining NDVI values from −0.15 to 0.10 thus represent grasses of low and high vitality. For the five plots, the median NDVI value of this alive grass vegetation was on average −0.11, hence we used this threshold to classify low-vitality grasses as those having NDVI values from −0.15 to −0.11, while high-vitality grasses ranged from −0.10 to 0.10.

We then inspected the 200 m × 200 m NDVI images and selected for each a 100 m × 100 m sub-window that was as much as possible devoid of shrub or tree aggregations given the study focus here was on the grasses. The 1-ha sub-windows thus represented the most homogeneous areas where grasses and FCs dominate. Unlike very young grasses that grow as separated individuals during the initial years, *T. basedowii* may form over time connected patches where individuals merge together and grow as one amalgamated unit, *c.* 1 m^2 in size (Figure 2c). For this reason, the NDVI images were resampled, based on the average NDVI value, into a raster layer

with 10,000 cells per hectare and grid cells of 1 m × 1 m resolution (Figure S2c), using QGIS-2.18 software (www.qgis.org). Finally, three NDVI classes for the 1 m^2 grid cells with *x*,*y*-coordinates were used for spatial statistical analyses: bare-soil cells (−0.37 to ≤−0.26), low-vitality grasses (−0.15 to −0.11) and high-vitality grasses (−0.10 to 0.10).

We then identified for the five 100 m × 100 m plots all FCs with a minimum threshold diameter of 2 m, using manual segmentation techniques as applied previously (Getzin et al., 2016; Getzin, Yizhaq, Munoz-Rojas, et al., 2019). Thus, for each FC we created with QGIS software one shapefile with geo-referenced information on the circle's *x*,*y*-coordinate and diameter. Smaller FCs were not considered because it is difficult to identify them as genuine FCs. The mean FC diameter in Australia is 4 m (Figure 2c), and it is these large FCs that are considered to function as an extra source of water for the surrounding vegetation.

2.4 | Spatial statistical analysis

2.4.1 | Spatial association of grass vitality with FCs and with all bare-soil gaps

The FCs are thought to create a hydraulically connected landscape and thereby affect the vitality of the grasses not only on a local scale but also as a large-scale landscape pattern of water availability (Cramer et al., 2017; Getzin et al., 2016; Tschinkel, 2015). We therefore used the Berman test (Berman, 1986) to investigate how far the density of low- and high-vitality grasses is associated with the spatially continuous covariate of water availability induced by run-off from the hardened FCs. To test the effect of this surrogate of water availability, the individual FC locations were converted into a kernel-smoothed covariate, using an Epanechnikov kernel with a radius of 5 m. Given that FCs in Australia have mean nearest-neighbour distances of 10 m (Getzin et al., 2016), a kernel radius of 5 m thus covers approximately the matrix vegetation half way to the neighbouring FC, and thereby the immediate area of the matrix vegetation that is most strongly affected by the nearest-neighbour FC (Figure S3).

In the Berman (1986) test, the observed distribution of the values S_{obs} of a spatial covariate *Z* at the grass data points *x* and the predicted distribution of the same covariate values S_{sim}, generated by 199 repeated simulations from the null model of complete spatial randomness (CSR), are compared using the Z_1 test statistic. Z_1 is computed based on the mean S_{obs} of the covariate values at all grass data points *x*: $Z_1 = (S_{obs} - \mu)/\sigma$ where μ is the mean value of S_{sim} under the null model and σ^2 the corresponding variance (Zhu, Getzin, Wiegand, Ren, & Ma, 2013). The null distribution of this test statistic is approximately the standard normal distribution. Based on this test statistic one can formulate the null and alternative hypotheses. H_0: *X* is a stationary Poisson point process independent of Z_1. H_1: conditionally on Z_1, the process *X* is an inhomogeneous Poisson point process with intensity depending on the distance from Z_1. We assessed significant deviation of the Z_1 scores from H_0 at $\alpha = 0.05$. Z_1-values between −1.96 and 1.96 correspond to a *p*-value >0.05 and encircle cases without significant departures of the null model. For each of the five FC plots, this test was done once only for the grid cells with low-vitality grasses and once only for the high-vitality grasses and then the Z_1 scores were compared (Figure S3). Note that Z_1 scores cannot attain positive values because the FC centre coordinates used to create the kernel-smoothed covariate are bare-soil locations, primarily without either low- or high-vitality grasses.

While the Berman test accounts for the large-scale landscape pattern of water availability induced by FCs, we also studied the immediate neighbourhood effect of all other bare-soil gaps on grass vitality, including small ones of just 1 m^2. We applied landscape metrics to these discrete land-cover classes (Hesselbarth, Sciaini, With, Wiegand, & Nowosad, 2019), i.e. we calculated the full adjacency matrix based on rook's case, where four directions around cells are considered as neighbours. The adjacency matrix thus describes the configuration of the landscape in the form of a cell-wise count of all edges between the classes of bare soil, low-vitality grasses and high-vitality grasses.

2.4.2 | Spatial patterns assessed with univariate random labelling

Finally, we were interested if the spatial patterns of high-vitality grasses differ from the patterns of low-vitality grasses and if these patterns show aggregated (clustered) or segregated (regular) distributions that correspond to the modelled positive and negative feedbacks at small and larger scales (Figure 1a). To test this formally, we applied the pair-correlation function (or short: *g*-function) and the null model of univariate random labelling (Wiegand & Moloney, 2004) once to the high-vitality and once to the low-vitality grasses. The $g(r)$ is a neighbourhood-density function that describes clumping and regularity at a given radius *r*, using a standardized density. It is the expected density of points at a given distance *r* of an arbitrary point, divided by the intensity λ of the pattern (Stoyan & Stoyan, 1994). Under complete spatial randomness, CSR, $g(r) = 1$, aggregation is indicated by $g(r) > 1$, while regularity has values of $g(r) < 1$. The function can be extended to describe point patterns with two types of points (e.g. low-vitality grasses = pattern 1, high-vitality grasses = pattern 2): the bivariate pair-correlation function $g_{12}(r)$ is the expected density of points of pattern 2 at distance *r* of an arbitrary point of pattern 1, divided by the intensity λ_2 of pattern 2.

Under random thinning the *g*-functions are invariant, hence under the null model of random labelling $g_{12}(r) = g_{21}(r) = g_{11}(r) = g_{22}(r)$. We used univariate random labelling as null model and the function $g_{11}(r)$ to explore if the low-vitality grasses (n_1) are a random subset of the overall grass pattern, i.e. the combined pattern of low-vitality (n_1) and high-vitality (n_2) grasses. The same was done for the high-vitality grasses (n_2), using the function $g_{22}(r)$. The test was applied by

computing the function $g_{11}(r)$ from the observed data, then randomly re-sampling sets of low-vitality grasses (or high-vitality grasses using $g_{22}(r)$, respectively) from the joined pattern of low-vitality and high-vitality grasses to generate the simulation envelopes. If the functions $g_{11}(r)$ or $g_{22}(r)$ show significant positive or negative deviations from the null model, this indicates that the low- or high-vitality grasses, respectively, have an additional clustered or regular spatial structure, conditional on the overall distribution of all grasses within the study plot. Univariate random labelling is an ideal null model to explore this question because it also accounts for first-order heterogeneity, i.e. non-relevant 1 m^2 grid cells with land-cover classes of bare soil or of trees and shrubs do not affect the spatial outcome of the analysis. Therefore, the null model envelopes reflect the first-order properties and, unlike for a CSR null model, are not parallel to a value of $g(r) = 1$. The spatial correlation functions $g_{11}(r)$ and $g_{22}(r)$ were tested for significant deviations from the null model using the fifth-lowest and fifth-highest values of 199 Monte Carlo simulations for constructing approximately 95% simulation envelopes (Baddeley et al., 2014). All spatial analyses were done in *R*-software using the packages 'SPATSTAT' (Baddeley & Turner, 2005) and 'LANDSCAPE METRICS' (Hesselbarth et al., 2019), as well as in the software Programita (Wiegand & Moloney, 2004).

2.5 | Quadrat-based mapping of post-fire succession

On 28th and 29th March 2019, we ground-mapped the number of individual *Triodia* grass hummocks and their cover in 1 m × 1 m sample quadrats. Three neighbouring, edaphically similar plots that represent different post-fire ages were chosen to monitor how these hummock grasses change their number and cover over time (Table S1; Figure S4). For this purpose, we used the FC-C2 plot because it burnt in early November 2014, hence its post-fire age was around 4.5 years in 2019. A new selected plot, named FC-F1, was just 700 m north of the FC-C2 plot and it burnt 3.5 years prior to March 2019. Since the nearby drone-mapped plots FC-L1, FC-L2, and FC-C5 burnt in April 2018, we could not use them as reference for vegetation in a climax stage. Instead, we selected a third plot about 300 m north of FC-F1, named FC-F3, that burnt >15 years ago. Post-fire age was identified using the FireWatch (https://firewatch-pro.landgate.wa.gov.au/) as in Muñoz-Rojas et al. (2016).

In each of the selected plots, 10 FCs that were connected along a transect were selected and the quadrat was placed at the north, west, south and east side of the peripheral vegetation, as well as at four neighbouring locations in the matrix vegetation, which were between 2 and 3 m away from the FC gap edge (Figure S4). The quadrat was subdivided into 10 cm × 10 cm subunits. For each quadrat, the number of individual, physically separated, grass plants per square metre was recorded (count), as well as their total crown cover within the square, which allowed to assess the cover precisely to 1%. The formula cover/count × 100 will thus attain a maximum value of 100 for a single large hummock grass occupying the full quadrat and it is therefore a measure of facilitation whereby small individual grasses merge together. To examine if cover and cover/count were significantly greater, and count smaller, at the edge of the FCs as compared to the matrix, the location effects between edge ($N = 40$) and matrix ($N = 40$), within the same post-fire age, were assessed with un-paired, one-tailed *t* tests. The age effects between the three plots, within the same locations ($N = 40$), were first assessed with analysis of variance (ANOVA), to test if cover, count or cover/count differ significantly. Afterwards, post-hoc Tukey tests were applied to test if these grass properties at the same locations ($N = 40$) differ significantly between pairs of individual post-fire ages. All three types of test were done in *R*-software, using a significance level of 5%.

2.6 | Installing a weather station

During the drone survey in 2017, we also installed a HOBO RX3000 Remote Monitoring Station with cellular network connectivity which is a solar-powered system that provides real-time access to the data from any web browser in the world. The purpose of setting up this data logger was to test if the FCs function as a source of water for the surrounding grasses and if there is the modelled infiltration contrast that shows more water percolation under plants with roots at the FC edge as compared to bare soil in the FC interior. A typical FC with about 5 m diameter was chosen in the climax vegetation of the plot FC-L2 to install at a depth of 5 cm six soil moisture sensors (S-SMD-M005) to measure volumetric soil-water content (SWC in m^3/m^3). One sensor was placed under bare soil inside the FC gap, 1.2 m away from the peripheral target plant which also had a sensor (cf. Section 3, Figure 7a). Another sensor was installed also under bare soil inside the FC, but only 30 cm away from the gap edge with the target plant. Two sensors were installed under alive and dead peripheral target plants, respectively, that directly border on the gap edge. A fifth sensor was installed under an alive plant 1.8 m away from the FC gap edge in the matrix vegetation. A sixth sensor was placed next to that plant but under bare soil in the matrix which was 2.5 m away from the gap edge. Additionally, two temperature sensors were installed at 2 cm depth next to the soil moisture sensor 1.2 m inside the gap and under the alive peripheral plant respectively. Furthermore, air temperature (°C) was measured at the HOBO station about 2 m above ground. These data were continuously recorded every 10 min between 4 August 2017 and 6 April 2018, when a strong fire interrupted the data logging in plot FC-L2. Nevertheless, the data recording represents the main dry and wet season.

3 | RESULTS

3.1 | Drone-based spatial analyses

The number of digitized FCs in the five 1-ha plots ranged between 81 and 105 (Table 1). Their diameters ranged between 2.0 and 5.9 m,

TABLE 1 Summary of the 1-ha plot properties as obtained from drone-based Normalized Difference Vegetation Index images with 10,000 cells per hectare and 1 m × 1 m resolution. The no. cells divided by 100 thus represents the coverage of the class in the plot. Further results are shown for the Berman test and the analysed adjacency matrix. Bold numbers of the Berman test indicate significant Z_1 scores with $p < 0.05$

	FC-L1	FC-L2	FC-C2	FC-C5	FC-1
Plot properties from drone imagery					
No. of FCs	105	81	81	92	87
Min Ø of FCs (m)	2.0	2.1	2.3	2.0	2.1
Mean Ø of FCs (m)	3.3	3.6	4.6	3.2	4.1
Max Ø of FCs (m)	4.9	5.4	5.9	5.0	5.8
No. of cells bare soil	1,333	1,521	1,683	1,122	2,053
No. of cells low-vitality grasses	2,344	2,379	1,479	2,000	1,775
No. of cells high-vitality grasses	1,206	1,151	1,964	1,750	1,342
Results from Berman test					
Z_1 score low-vitality grasses	**−5.134**	**−5.502**	**−7.751**	**−5.005**	**−7.134**
Z_1 score high-vitality grasses	−1.104	**−2.985**	**−4.88**	**−4.231**	**−5.985**
Results from adjacency matrix					
% low-vitality grasses next to bare soil	42.3	42.8	48.5	34.7	51.0
% high-vitality grasses next to bare soil	34.6	36.0	39.0	22.9	36.4

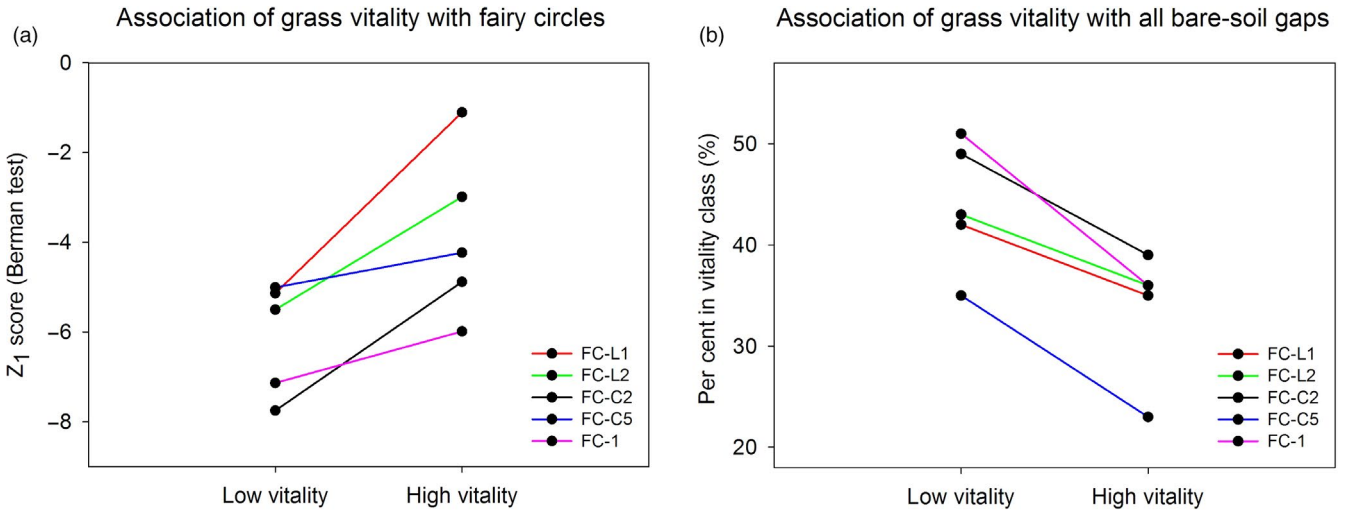

FIGURE 3 Graphical presentation of the Z_1 scores from the Berman tests (a), as shown in Table 1. High-vitality grasses had consistently higher Z_1 scores than low-vitality grasses, thus demonstrating a stronger association with the FCs. An opposite relationship is shown for results with the adjacency matrix (b), which considered all small gaps up to a minimum size of 1 m^2, revealing that the proportion of low-vitality grasses bordering a bare-soil gap was higher than for the high-vitality grasses

with an overall mean diameter of 3.8 m. Of all the 10,000 cells per hectare, the number of cells representing bare soil ranged between 1,122 and 2,053 or 11.2% and 20.5% respectively. Generally, there were more low-vitality than high-vitality grasses in the plots, except for the very young plot FC-C2 where an opposite relation occurred. Approximately 50% of all cells were classified as either trees or shrubs with very high NDVI values or as 'noise', showing a transition from bare soil towards coverage with varying proportions of dead lignified grasses and litter.

The Berman tests showed consistent trends for all five plots. Low-vitality grasses always had lower Z_1 scores and thus a lower spatial association with the 81–105 FCs than high-vitality grasses (Table 1; Figure 3a). The density of high-vitality grasses was therefore more positively affected by the distribution of FCs than the density of low-vitality grasses. These results were robust because they were the same when we used in an additional analysis not the median but the mean NDVI value (−0.10) of all five plots to differentiate between low- and high-vitality grasses (Figure S5a).

In contrast to the Berman test which focuses on the effect of FC gaps with diameters ≥2 m, if all bare-soil cells in a plot such as FCs and gaps up to a minimum size of 1 m^2 are assessed via the adjacency

matrix, the percentage of high-vitality grasses bordering a bare-soil cell was consistently lower than for the low-vitality grasses (Table 1; Figure 3b). Smallest gap openings thus had no positive effect on grass vitality.

Spatial patterns assessed with the null model of univariate random labelling revealed that high-vitality grasses in all five plots were consistently aggregated at the first neighbourhood scales. This significant clustering effect was strong for four plots, showing large deviations from the null model, but weak for the young FC-C2 plot which burnt 2 years and 8 months ago, prior to the drone survey in 2017 (Figure 4). The clustering of high-vitality grasses was particularly strong for the smallest scale of 1 m radius, with g_{22}-values ranging between 1.65 and 1.86 in the four long unburnt plots. The absolute difference between the g_{22} values and the upper simulation envelope was consistently largest for the smallest scale of 1 m, reaching differences of 0.49, 0.55, 0.09, 0.42, 0.49 for the plots FC-L1, FC-L2, FC-C2, FC-C5, FC-1 respectively. Both, the high g_{22} values and the large positive deviations from the upper null-model envelopes, indicate strong facilitation of the grasses at smallest scales.

In contrast, all low-vitality grasses did not show positive deviations from the null model. Here, mostly regularity was detected and this regularity was just marginally significant at the smallest scales of $r \leq 2$ m (Figure 4a,b,e, inset). In the youngest plot FC-C2, low-vitality grasses showed even random distributions at the smallest scales. Unlike the high-vitality grasses, which show strong facilitation with their positive small-scale deviation from the null model, the low-vitality grasses had their largest absolute difference between the g_{11} values and the lower simulation envelope not at the 1-m scale but often at larger scales, e.g. at 8 m in FC-C2 or at 2 m in the plots FC-C5 and FC-1. This indicates that negative feedbacks and competition occurred only within the low-vitality grasses and it prevailed at larger scales. These negative deviations from the lower simulation envelopes reached only values of 0.05, 0.05, 0.03, 0.07, 0.06 for the plots FC-L1, FC-L2, FC-C2, FC-C5, FC-1, respectively, indicating a lower negative feedback strength, as compared to the strong positive feedback exerted by the high-vitality grasses. Thus, high-vitality grasses exerted a very strong positive feedback at shortest distances and the low-vitality grasses a weaker negative feedback at longer distances (cf. Figure S6).

3.2 | Quadrat-based analyses of post-fire succession

Grass cover in the 1 m^2 sample quadrats was significantly smaller in the matrix locations than at the FC edge in all three age groups

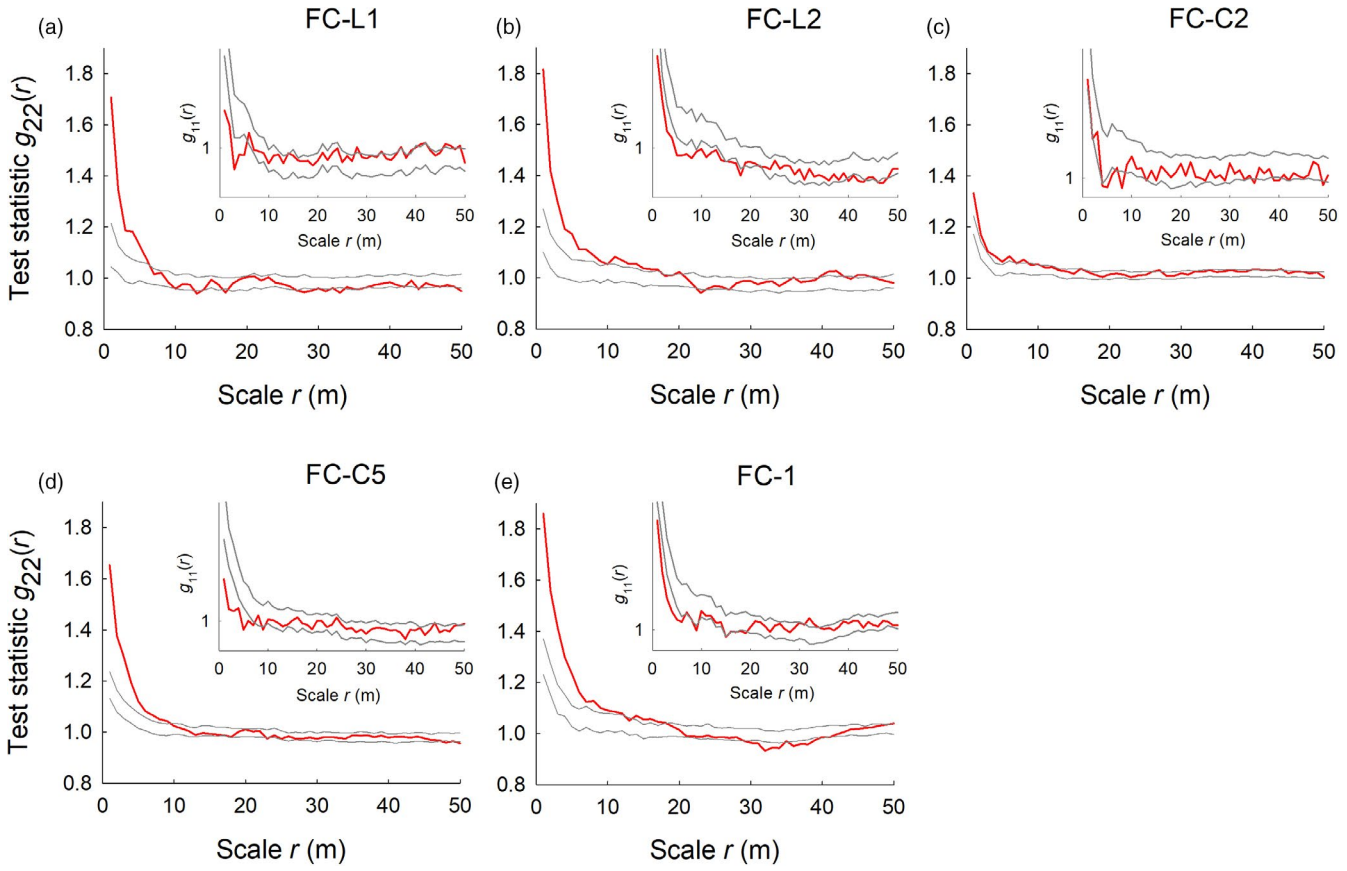

FIGURE 4 Spatial patterns of grasses in the five 1-ha plots assessed with the null model of univariate random labelling, once shown for the high-vitality grasses, denoted g_{22}, and once for the low-vitality grasses, g_{11} (inset figure). The pattern is regular or aggregated at circular neighbourhood distances if the red line of the g-function is either below the lower or above the upper grey lines of the simulation envelopes respectively. Envelopes were constructed using the 5th lowest and 5th highest value of 199 Monte Carlo simulations of the null model

of 3.5, 4.5 and >15 years after fire. At the FC edge, grass cover increased significantly with post-fire age (Table 2; Figure 5a). In the matrix, grass cover also increased significantly with post-fire age except that there was no significant difference between the very young FC-F1 and FC-C2 plots. This indicates that the positive effect of the FC on plant growth most strongly benefitted the grasses growing directly on the FC edge. Between the edge and matrix locations, count was only significantly smaller at the FC edge for the very young FC-F1 plot. The number of individual grass hummocks significantly decreased with post-fire age within the same locations (Table 2; Figure 5b). The best measure to describe the merging of small individual grasses into self-organized patches (i.e. large hummocks) is cover/count × 100 because it would give a value of 100 for complete coverage with one plant. This measure was significantly smaller in the matrix locations than at the FC edge in all age groups (Table 2). Overall, it also increased with post-fire age (Figure 5c).

3.3 | Weather station data

The highest recorded air temperature between 4 August 2017 and 6 April 2018 was 48.2°C on 6 January 2018. Seven more days occurred

TABLE 2 Details of the quadrat-based measurements, shown in Figure 5. The location effects within plots, edge versus matrix, were examined with one-tailed *t* tests to analyse if cover and cover/count were significantly greater at the edge or if count was significantly smaller at the edge. The age effects among the three plots were first assessed with analysis of variance (ANOVA), and then with post-hoc Tukey tests to analyse if cover, count or cover/count differ significantly for different post-fire ages. Bold numbers indicate significant test results with $p < 0.05$

	Location effect, *t* test	Mean	*t* Value	*p*-Value	Age effect, ANOVA	*F*-value	*p*-Value	Age effect, Tukey test	Diff. in means	*p*-Value
Cover (%)	FC-F1 Edge	33.1	2.630	**0.005**	FC-F1 Edge	61.51	**<0.001**	FC-F1 versus FC-C2	−9.2	**0.026**
	FC-F1 Matrix	27.5			FC-C2 Edge			FC-F3 versus FC-C2	28.0	**<0.001**
	FC-C2 Edge	42.2	3.806	**<0.001**	FC-F3 Edge			FC-F3 versus FC-F1	37.2	**<0.001**
	FC-C2 Matrix	29.2			FC-F1 Matrix	28.82	**<0.001**	FC-F1 versus FC-C2	−1.7	0.920
	FC-F3 Edge	70.2	2.503	**0.007**	FC-C2 Matrix			FC-F3 versus FC-C2	27.4	**<0.001**
	FC-F3 Matrix	56.6			FC-F3 Matrix			FC-F3 versus FC-F1	29.1	**<0.001**
Count	FC-F1 Edge	5.7	−2.696	**0.004**	FC-F1 Edge	84.64	**<0.001**	FC-F1 versus FC-C2	2.0	**<0.001**
	FC-F1 Matrix	7.1			FC-C2 Edge			FC-F3 versus FC-C2	−2.2	**<0.001**
	FC-C2 Edge	3.7	0.398	0.654	FC-F3 Edge			FC-F3 versus FC-F1	−4.2	**<0.001**
	FC-C2 Matrix	3.6			FC-F1 Matrix	96.48	**<0.001**	FC-F1 versus FC-C2	3.6	**<0.001**
	FC-F3 Edge	1.5	0.482	0.684	FC-C2 Matrix			FC-F3 versus FC-C2	−2.2	**<0.001**
	FC-F3 Matrix	1.4			FC-F3 Matrix			FC-F3 versus FC-F1	−5.7	**<0.001**
Cover/count (%)	FC-F1 Edge	6.4	4.358	**<0.001**	FC-F1 Edge	108.4	**<0.001**	FC-F1 versus FC-C2	−6.4	0.212
	FC-F1 Matrix	4.2			FC-C2 Edge			FC-F3 versus FC-C2	44.5	**<0.001**
	FC-C2 Edge	12.8	3.053	**0.002**	FC-F3 Edge			FC-F3 versus FC-F1	50.8	**<0.001**
	FC-C2 Matrix	8.3			FC-F1 Matrix	64.24	**<0.001**	FC-F1 versus FC-C2	−4.1	0.561
	FC-F3 Edge	57.2	1.787	**0.039**	FC-C2 Matrix			FC-F3 versus FC-C2	37.2	**<0.001**
	FC-F3 Matrix	45.5			FC-F3 Matrix			FC-F3 versus FC-F1	41.3	**<0.001**

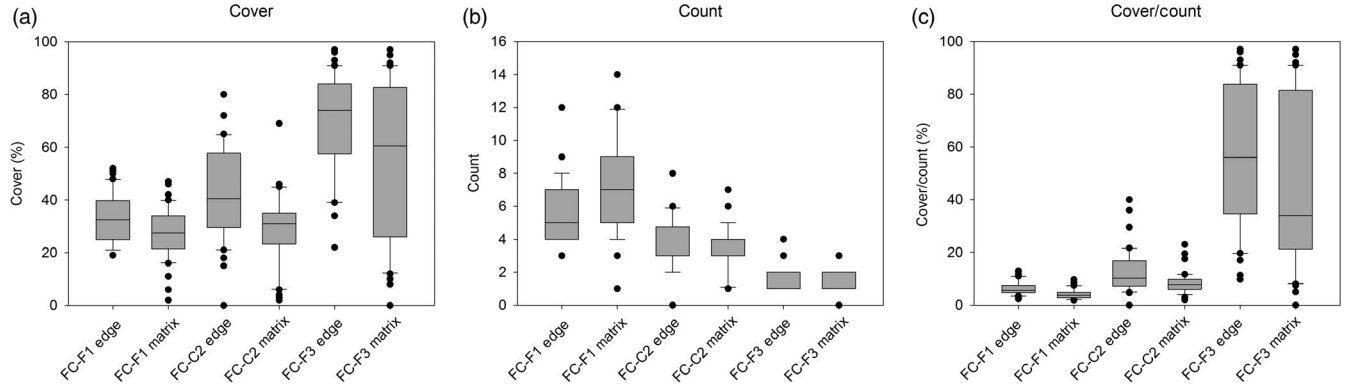

FIGURE 5 Results from the quadrat-based fieldwork for the three plots with different post-fire age. The plots FC-F1, FC-C2 and FC-F3 burnt 3.5, 4.5 and >15 years ago respectively. Cover increased with post-fire age and was highest at the FC edge (a). Similarly, the number of individual plants declined (b). The statistic count/cover shows that grasses were increasingly merging together with increased post-fire age and at the FC edge (c)

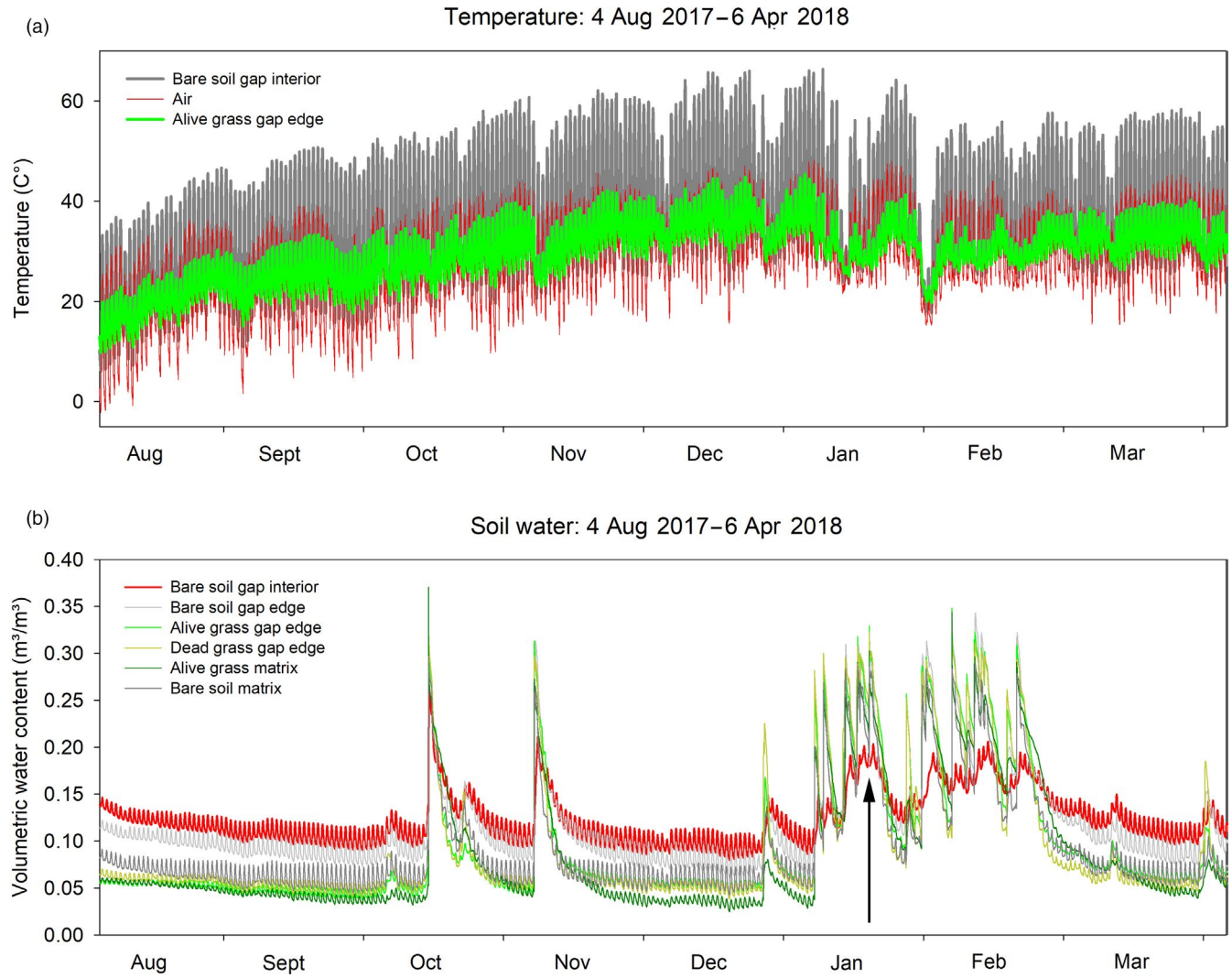

FIGURE 6 Measured soil temperature at 2 cm depth under alive grass at the FC gap edge and in bare soil of the gap interior, and corresponding air temperature (a). Volumetric water content at the six soil moisture sensors within and around the FCs (b). The lines of the legend are sorted according to the positions of the sensors, starting from the FC gap interior outwards to bare soil in the matrix. The black arrow indicates that soil water of only the sensor in the FC gap interior (red line) showed decreased soil water in mid-January, which can be attributed to physical weathering and the re-establishment of the soil crust during the rainfall events in the months before. Note that soil moisture values had different absolute values during non-rainfall times due to differences in the initial calibration

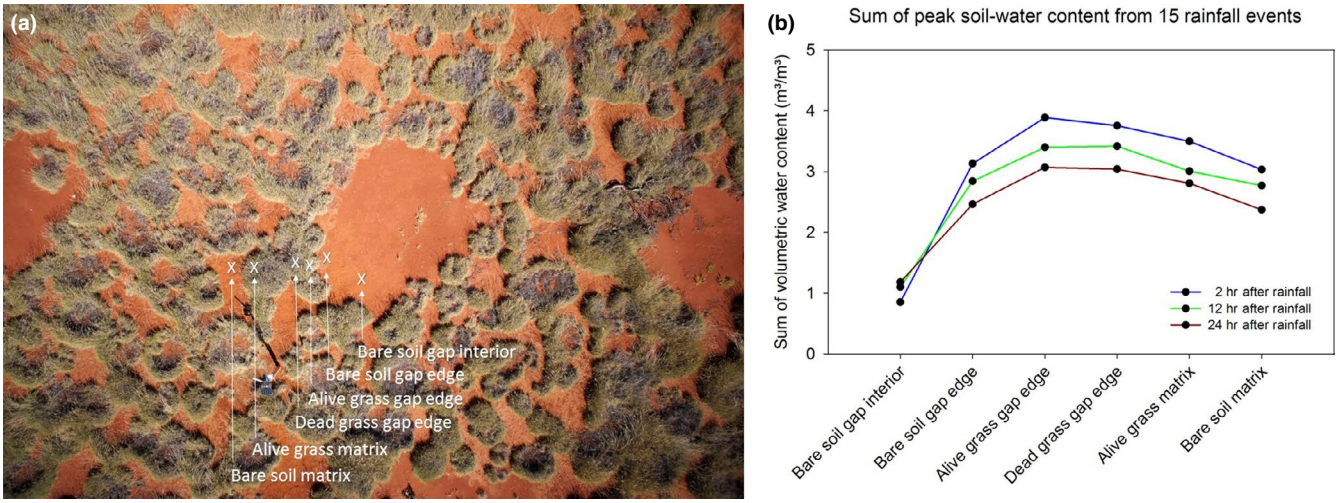

FIGURE 7 Drone image of the weather station and the positions of the soil moisture sensors (a). Sum of the peak soil-water content 2, 12, and 24 hr after rainfall, accumulated over 15 rainfall events (b). Soil–water content was highest under the alive grass plant at the gap edge but lowest in the FC gap interior

between December 2017 and January 2018 when air temperature exceeded 47°C. The lowest air temperature was −2.3°C, recorded on 4 August 2017. The highest soil temperature at 2 cm depth occurred with 66.4°C on 8 January 2018 in the interior of the FC gap, while the corresponding soil temperature under the alive peripheral plant was only 41.3°C at that time (Figure 6a). The protective plant cover could thus reduce soil surface temperatures by about 25°C at the hottest time of the day between 1 and 3 p.m.

In total, there were 15 rainfall events, occurring between October 2017 and February 2018, when the volumetric soil-water content (SWC) of at least one sensor exceeded 0.25 m^3/m^3. These rainfall events revealed two main findings. First, SWC of only the sensor in the FC gap interior strongly decreased during the very hot January, after several major rainfall events during the previous months (Figure 6b, black arrow). This indicates that the initial mechanical surface crust in the unprotected FC gap has quickly reformed after the disturbance caused by installation of the sensor. Second, the peak SWC 2, 12 and 24 hr after rainfall was highest under the alive plant at the FC gap edge but lowest in the gap interior (Figure 7). SWC decreased from the alive plant of the FC gap edge towards the matrix locations about 2–2.5 m distance away from the FC. Only for the interior of the FC gap, SWC was higher 12 and 24 hr after rainfall than 2 hr after rain, indicating that immediate water infiltration in the FC gap was low. These results represent standardized values of peak soil-water content, i.e. the initial differences in calibration of the six sensors during the dry season and their mean values from 3 days (26–28 September, Figure 6b) were subtracted from the peak values.

4 | DISCUSSION

With this study, we are quantitatively testing whether the theoretically assumed, scale-dependent feedback mechanisms and modes of water transport are valid for modelling the emergent patterns of Australian FCs. Generally, it is not enough to show that the modelled high-order components, such as the spatially periodic FCs patterns, are statistically well matched by the real-world patterns observed in aerial imagery. This is because several modes of water transport and different feedback mechanisms of plant self-organization can lead to periodic vegetation patterns (Meron, 2015, 2016; Rietkerk & van de Koppel, 2008). If the process-based partial-differential equation models that are rooted in physics and in pattern-formation theory shall find greater acceptance in ecology, then it is necessary to verify beyond these coarse-graining properties that the a priori assumed lower-level feedback processes are indeed explaining the emergent vegetation patterns (Newman et al., 2019). Here we have taken up this challenge and provide one of the rare studies on spatially periodic dryland vegetation that examines the modelled processes in the field. We combine within a holistic framework several types of empirical work to test (a) if the grasses systematically benefit from the FCs in the landscape, (b) if facilitation and competition of grasses reflects scale-dependent positive and negative feedbacks and (c) if spatio-temporal soil-water content is in accordance with the modelled infiltration feedback.

4.1 | Landscape-scale feedbacks of grasses and their association with FCs—*Hypothesis 1*

According to pattern-formation theory, the periodically ordered FCs are not a random event but are inherently linked to the demography of the grass population. In *Triodia* grasslands with climax vegetation, healthy grasses of high vitality should therefore show a stronger spatial association with the FCs than low-vitality grasses since they should benefit from surface water flow from the gap interior to the edges. We examined this hypothesis with a drone survey during the driest month of the year with zero rainfall in July and June, and only 11 mm in May 2017 (data

for Newman Airport, Australian Government Bureau of Meteorology, 2018). As a consequence and based on the NDVI, we found generally more low-vitality than high-vitality grasses in the plots. Only in the very young plot FC-C2, which burnt 2 years and 8 months prior to the drone survey in July 2017, we found an opposite relationship because the smaller plants were likely not strongly constrained by intraspecific competition and resultant mortality. Given that the other drone-mapped plots represent typical climax stages of *Triodia* grassland, it is not surprising that a considerable proportion of the 1-ha plots consisted of bare soil-litter transitions with variable amounts of dead lignified grasses. The perennial grass species *T. basedowii* grows permanently until neighbourhood competition, resource depletion or the central collapse of a hummock leads to plant death or ring formation. Hence, if fire is absent for a long time, considerable amounts of dead leaf material within hummocks accumulate (Grigg et al., 2008) and this increase of combustible material increases the probability of fire (Haydon, Friar, & Pianka, 2000). The research plots FC-L1, FC-L2 and FC-C5 that had not burnt for >15 years, were likely in a terminal phase of this successional stage because their entire grass layers burnt in April 2018 due to a wildfire.

In these plots with climax vegetation, but even in the young plot FC-C2, high- and low-vitality grasses responded systematically to the pattern of FCs. Based on the spatially explicit Berman test, we found that the high-vitality grasses of all five investigated plots were consistently more strongly associated with the surrounding FCs than the low-vitality grasses (Figure 3a). This is a strong indication that the grasses that grow closer to the FCs must have benefited from these large gaps, which have mean diameters of nearly 4 m in the study region, equalling an area of about 12 m^2 (Getzin et al., 2016). Since this result is based on a spatially explicit test, it reflects the positive response of all high-vitality grasses in the 1-ha study plot, no matter whether they grow near the periphery of the FC gap or at distances of some metres away from the FCs. These results were also robust when we used the mean NDVI value rather than the median as cut-off value to differentiate between low- and high-vitality grasses. Our analysis also shows that the Epanechnikov kernel is more suitable than a Gaussian kernel to account for the relationship between FCs and grass vitality because its parabolic shape depicts more clearly the direct neighbourhood effect of FCs on the surrounding vegetation half way to the next FC. Expectedly, kernel radii larger than 5 m include too much noise effects from other nearby FCs and therefore result in inconsistent and non-significant results (Figure S5).

In contrast, if the adjacency matrix is assessed, which considers all FCs and all bare-soil gaps in the area down to a minimum size of 1 m^2, then an opposite relation can be found. In this case, the percentage of low-vitality grasses bordering a bare-soil gap was consistently higher than for the high-vitality grasses. This indicates that not every small gap is necessarily important for the demography of the *Triodia* grasses. In other words, the potential positive effect of less neighbourhood competition from growing randomly next to a small bare-soil gap could be functionally unimportant, relative to the overall constraint that the demographics of this highly water-limited grassland system is governed by the wavelength of the FCs at the landscape-scale and the geometric rules of pattern-formation theory (Deblauwe et al., 2008; Getzin et al., 2016; Meron et al., 2004; Rietkerk & van de Koppel, 2008). Also, small gaps which occur in the matrix are likely those places which receive less water from the FCs. Consequently, continuous plant cover cannot be sustained in the matrix and small gaps form.

The FCs are distributed in a spatially periodic pattern and, as predicted by pattern-formation theory, form a grid-like hexagonal array (Getzin, Yizhaq, Cramer, et al., 2019). Our empirical results thus support the theoretical model assumptions based on the reaction-diffusion principle and scale-dependent feedbacks where the hardened FC gaps function as an important additional source of water for the surrounding vegetation matrix (Getzin et al., 2016; Meron, 2018).

4.2 | Scale-dependent feedbacks, facilitation and competition of grasses—*Hypothesis 2*

Grasses of the matrix in-between FCs have already been investigated in previous studies (Cramer et al., 2017; Ravi et al., 2017; Tarnita et al., 2017), but the spatially explicit analysis of their vitality status is a novel approach. The Australian outback is an ideal ecosystem to study scale-dependent feedbacks of grasses because *T. basedowii* is a long-lived perennial that grows in size for years and decades until fire destroys the vegetation (Levin et al., 2012). High-vitality grasses which primarily exert positive short-range feedbacks should have clustered distributions and increasingly merge at the FC gap edge to increase their benefit from higher water availability. But low-vitality grasses which suffer from long-range negative feedbacks, should not have clustered but segregated or scattered random distributions because the lack of water does only support the survival of separate individuals. Our results support this model assumption based on univariate random labelling and fine-scale quadrat sampling.

High-vitality grasses were in all five plots significantly aggregated and the small-scale clustering at 1 m neighbourhood distance was particularly strong in the four long unburnt plots with g_{22} values ranging between 1.65 and 1.86. This aggregation is indicative of a strong positive short-range feedback where the more vital grasses not only benefit from the nearby FC gaps but also from a clustered growth pattern and resultant self-organized patch formation due to facilitation (Rietkerk et al., 2004). The reason for the clustered pattern of vital grasses can be found, for example, in a reduction of temperature under grass canopy versus bare soil. In our study area, soil surface temperature under grass shade was up to 25°C lower than in unshaded bare soil (Figure 6a). Also, enhanced trapping of sediments or organic detritus may trigger the increase in local density of grasses and thereby the increase in water-trapping efficiency among the grasses (Dunkerley & Brown, 1999). In such densely vegetated areas, the protection against evapotranspiration and against soil-crust formation enhances surface water infiltration which, in turn, favours vegetation growth. Thereby, the grasses redistribute the water resources, they modulate the abiotic environment and thus function as 'ecosystem engineers' to better cope with the hostile habitat (Borgogno et al., 2009; Gilad et al., 2004). Generally,

such facilitative patterns are well known to become increasingly important under increasing xeric conditions and in this case the positive effects of nurse shade outweigh competitive negative effects (Holmgren, Scheffer, & Huston, 1997). However, within such a competition–facilitation trade-off, the positive effects of nurse shade can only function if there is the demonstrated positive net-effect of the FC gaps on grass vitality.

With the assessment of the g_{11}-function and its low absolute deviations from the lower null-model envelopes (Figure 4), we found that low-vitality grasses showed a weaker feedback strength than high-vitality grasses with their strong positive deviations from the null model. This negative feedback, which indicates competition between plants, prevailed at larger scales than the positive feedback of facilitating high-vitality grasses. In terms of multiple-scale feedbacks, this agrees strongly with the central model assumption that positive feedbacks and facilitation should act at short distances, while negative feedbacks resulting from competition for resources should act at larger distances (Figure 1a; Rietkerk & van de Koppel, 2008). With regard to these different feedback strengths, our empirical results specifically agree with the conceptual figure of Borgogno et al. (2009) and indicate that the feedback strength should be greater at small scales than at larger scales (Figure S6). This is because facilitation occurs mainly in the immediate neighbourhood around plant crowns while competitive negative plant interaction happens more at the larger scale of plant roots, and ultimately the feedback strength vanishes with further distances between plants. Overall, our spatially explicit results from univariate random labelling confirm the presence of short-range positive and long-range negative feedbacks that have been used to model the Australian FCs.

The scale-dependent feedbacks and facilitation of grasses also become evident from the fine-scale mapping around the FCs. Mature *Triodia* grasses under climax conditions have typical plant sizes of 1 m^2 and more (Figure 2c). While our drone-based analysis has accounted for the growth pattern of these typical hummocks via the 1 m^2 grid resolution, we also mapped the post-fire grass recovery of young hummocks within 1 m^2 sample quadrats that were subdivided into 10 cm × 10 cm subunits.

Our ground mapping supports those drone-based findings because we found a spatio-temporal trend that plant cover bordering the FC edge was higher than for the matrix grasses at distances of 2–3 m away from the gap edge. This trend became more prominent with increasing post-fire age from 3.5 years towards >15 years (Figure 5a), indicating that the increase in plant cover around the FCs follows a demographic rule: the highest coverage forms directly around the FC edges, while off the FCs the plant cover is lower and the probability of gap formation between the hummocks increases. Corresponding to these findings, the number of individual grass hummocks declined in a similar way and the cover/count statistic shows that the cooperative merging of grass individuals increased towards the FC edge but also with post-fire age. These results provide additional evidence that the grasses are overall benefiting from the FCs that function as an important extra source of water and that the trend of facilitation via the merging of seed-regenerating grass individuals was positively associated with the decreasing distance to the FC gaps (Getzin et al., 2016; Meron, 2018). With their population-level response to aridity stress the *Triodia* grasses act as ecosystem engineers and the morphological plasticity in their growth patterns are adaptations to maximize water harvesting (Figure S4g–j). Such morphological adaptations of grass plants are well known from a number of water-limited environments and include, for example, the formation of ring-like shapes (Sheffer, Yizhaq, Gilad, Shachak, & Meron, 2007; Yizhaq et al., 2019), spiral-like (Fernandez-Oto, Escaff, & Cisternas, 2019) or banded grass patterns (Dunkerley, 2018; Dunkerley & Brown, 1999) and high grass biomass of the perennial belt around FCs in Namibia (Cramer et al., 2017; Fernandez-Oto, Tlidi, Escaff, & Clerc, 2014).

4.3 | Spatio-temporal data recording of a weather station and the infiltration feedback—*Hypothesis 3*

Central to the process-based modelling of the FCs is a Turing-like instability that is triggered by a specific feedback mechanism and mode of water transport which depend on the prevailing soil type and dominant plant architecture. While in Namibia on deep aeolian sand it is the 'uptake-diffusion feedback' that is assumed to induce the instability, in Australia on hardened clay crusts and associated overland-water flow it is the 'infiltration feedback' (Getzin et al., 2016; Zelnik et al., 2015). Consequently, the pivotal process for modelling the emergent pattern of the Australian FCs is enhanced soil-water infiltration under alive plants growing next to the hardened FCs gaps. The positive short-range feedback loop is thus triggered by the growth of roots that loosen the soil crusts and increase vegetation growth via locally taking up more water. Here we provide empirical evidence that this assumed mechanism of water transport is indeed existing in the studied grassland system. In this regard, the results of our installed data loggers show two important findings:

First, soil water only at the sensor in the FC gap without protective plant cover strongly decreased over time during the very hot January, after several major rainfall events happened during the months before (Figure 6b). This demonstrates that the soil crusts in the FCs originate from particle dispersion during heavy rainfall events and subsequent mechanical weathering of the soil surface under the extremely hot temperatures, which ultimately prevent plant establishment (Getzin et al., 2016). With more than 150 excavations in the Australian FCs, it has been previously shown that pavement termitaria are not responsible for the bare soil in FCs, but it is the high clay content and associated high soil compaction, induced by mechanical weathering, that is causing the absence of vegetation in FCs and similarly in nearby large bare-soil areas (Getzin, Yizhaq, Munoz-Rojas, et al., 2019), just like in many more Australian drylands (Dunkerley, 2002).

Second, the modelled infiltration feedback is supported by the observation that the peak soil-water content 2, 12 and 24 hr after rainfall was highest under the alive plant at the gap edge but lowest in the gap interior. Soil-water then decreased with larger scales from the alive plant at the FC edge towards the matrix locations about 2–2.5 m distance away. This shows further that the FC gaps function as an additional source of water for the matrix grasses and that it is the plants

growing close to the FCs that are benefiting the most from this water source. These findings are in line with previous infiltration measures and an irrigation experiment within a FC (Getzin et al., 2016) and the field results support the assumed in-phase spatial profiles of biomass and soil water of the model (Figure S1). The results can also explain why the grasses around the gap edge are merging together because a nearly closed barrier around the FCs minimizes the outflow of water from the gap towards the matrix plants. This population-level response to water stress and the positive net-effect of facilitation also explains why the high-vitality grasses are strongly associated with the FCs and why they can afford to have clustered distributions, while at the same time the low-vitality grasses at further distances are struggling as segregated or randomly scattered entities.

5 | CONCLUSIONS

Bridging empirical ecology and physics is one of the most challenging, but also most interesting, endeavours in the natural sciences. Such multi-disciplinary research efforts usually take time due to different types of commonly used language or terminology but also due to finding a general acceptance of each other within the two fields of science. Here, we demonstrate exemplarily based on the striking Australian fairy circles, how modelling and a priori assumed processes can be verified using detailed ecological fieldwork.

Our findings support the presence of ecohydrological feedbacks at the landscape-scale and at the scale of the immediate plant neighbourhood that are central to explain this emergent grassland gap pattern via Turing dynamics and pattern-formation theory. We have provided multiple-scale evidence that the grasses with their cooperative growth dynamics function as ecosystem engineers. Thereby, they modulate the abiotic environment to better cope with the permanent shortage of water in this arid ecosystem. The empirically found short-range positive and long-range negative feedbacks between the plants, the relative feedback strengths and the infiltration contrast all agree with the theoretical assumptions used for modelling the FCs based on Turing dynamics and the reaction-diffusion mechanism.

We conclude that by forming periodic gap patterns, the vegetation benefits from the additional water resource provided by the FC gaps, and thereby keeps the ecosystem functional at lower precipitation values compared with uniform vegetation (Meron, 2018). More field studies are needed for a more complete validation of the mathematical models of FCs and to enable a more realistic parameterization. Especially investigating the time scales of pattern formation in this dryland deserves more research because such patterns may be very long lived and form over hundreds of years (Caviedes-Voullième & Hinz, 2020). In this way, mutual collaboration between empiricists and modellers, for example with backgrounds in physics and ecology, will lead to a deep understanding of multi-scale feedbacks in complex ecological systems.

ACKNOWLEDGEMENTS

We thank Scott Duffy and the CASA/Aviation Group for permitting us to undertake the drone flights. We are grateful to the drone company Microdrones in Germany for their technical support, supplying us with new batteries. We thank BHP Western Australia Iron Ore, Rio Tinto and Barry Gratte from Ethel Creek Company for the permit to undertake fieldwork on their land. Bronwyn Bell and Lawrence Billson are thanked for their help in Perth and Emma Stock for assistance in the Pilbara. We are grateful to the German Research Foundation (DFG) for supporting this research project no. 323093723 and two anonymous reviewers for their constructive suggestions to improve the manuscript. Open access funding enabled and organized by Projekt DEAL.

AUTHORS' CONTRIBUTIONS

S.G., T.E.E. and H.Y. conceptualized the study and designed the methodology; S.G., T.E.E., H.Y. and M.M.-R. collected the data; S.G., T.E.E. and H.Y. analysed the data; S.G., T.E.E., H.Y., M.M.-R., A.H. and K.W. wrote the paper. All authors contributed critically to the drafts and gave final approval for publication.

PEER REVIEW

The peer review history for this article is available at https://publons.com/publon/10.1111/1365-2745.13493.

DATA AVAILABILITY STATEMENT

All data used for the presented results are provided as CSV files and can be downloaded from Zenodo https://doi.org/10.5281/zenodo.3979233 (Getzin et al., 2020). Other raw data are confidential, as they are subject to ongoing publications.

ORCID

Stephan Getzin https://orcid.org/0000-0003-4035-4834
Todd E. Erickson https://orcid.org/0000-0003-4537-0251
Miriam Muñoz-Rojas https://orcid.org/0000-0002-9746-5191

REFERENCES

Acharya, S., Kaplan, D. A., Casey, S., Cohen, M. J., & Jawitz, J. W. (2015). Coupled local facilitation and global hydrologic inhibition drive landscape geometry in a patterned peatland. *Hydrology and Earth System Sciences*, *19*, 2133–2144. https://doi.org/10.5194/hess-19-2133-2015

Australian Government Bureau of Meteorology. (2018). *Climate statistics for Australian locations*. Retrieved from http://www.bom.gov.au/climate/averages/tables/cw_007176.shtml

Baddeley, A., Diggle, P. J., Hardegen, A., Lawrence, T., Milne, R. K., & Nair, G. (2014). On tests of spatial pattern based on simulation envelopes. *Ecological Monographs*, *84*, 477–489. https://doi.org/10.1890/13-2042.1

Baddeley, A., & Turner, R. (2005). Spatstat: An R package for analyzing spatial point patterns. *Journal of Statistical Software*, *12*, 1–42. https://doi.org/10.18637/jss.v012.i06

Barbier, N., Couteron, P., Lefever, R., Deblauwe, V., & Lejeune, O. (2008). Spatial decoupling of facilitation and competition at the origin of gapped vegetation patterns. *Ecology*, *89*, 1521–1531. https://doi.org/10.1890/07-0365.1

Berman, M. (1986). Testing for spatial association between a point process and another stochastic process. *Applied Statistics*, *35*, 54–62. https://doi.org/10.2307/2347865

Boaler, S. B., & Hodge, C. A. H. (1962). Vegetation stripes in Somaliland. *Journal of Ecology*, *50*, 465–474. https://doi.org/10.2307/2257565

Borgogno, F., D'Odorico, P., Laio, F., & Ridolfi, L. (2009). Mathematical models of vegetation pattern formation in ecohydrology. *Reviews of Geophysics*, *47*, RG1005. https://doi.org/10.1029/2007RG000256

Caviedes-Voullième, D., & Hinz, C. (2020). From nonequilibrium initial conditions to steady dryland vegetation patterns: How trajectories matter. *Ecohydrology*, *13*, e2199. https://doi.org/10.1002/eco.2199

Couteron, P., & Lejeune, O. (2001). Periodic spotted patterns in semi-arid vegetation explained by a propagation-inhibition model. *Journal of Ecology*, *89*, 616–628. https://doi.org/10.1046/j.0022-0477.2001.00588.x

Cramer, M. D., & Barger, N. N. (2013). Are Namibian 'fairy circles' the consequence of self-organizing spatial vegetation patterning? *PLoS ONE*, *8*, e70876. https://doi.org/10.1371/journal.pone.0070876

Cramer, M. D., Barger, N. N., & Tschinkel, W. R. (2017). Edaphic properties enable facilitative and competitive interactions resulting in fairy circle formation. *Ecography*, *40*, 1210–1220. https://doi.org/10.1111/ecog.02461

Deblauwe, V., Barbier, N., Couteron, P., Lejeune, O., & Bogaert, J. (2008). The global biogeography of semiarid periodic vegetation patterns. *Global Ecology and Biogeography*, *17*, 715–723. https://doi.org/10.1111/j.1466-8238.2008.00413.x

Deblauwe, V., Couteron, P., Lejeune, O., Bogaert, J., & Barbier, N. (2011). Environmental modulation of self-organized periodic vegetation patterns in Sudan. *Ecography*, *34*, 990–1001. https://doi.org/10.1111/j.1600-0587.2010.06694.x

Dunkerley, D. L. (2002). Infiltration rates and soil moisture in a groved mulga community near Alice Springs, arid central Australia: Evidence for complex internal rainwater redistribution in a runoff–runon landscape. *Journal of Arid Environments*, *51*, 199–219. https://doi.org/10.1006/jare.2001.0941

Dunkerley, D. (2018). Banded vegetation in some Australian semi-arid landscapes: 20 years of field observations to support the development and evaluation of numerical models of vegetation pattern evolution. *Desert*, *23*, 165–187.

Dunkerley, D. L., & Brown, K. J. (1999). Banded vegetation near Broken Hill, Australia: Significance of surface roughness and soil physical properties. *Catena*, *37*, 75–88. https://doi.org/10.1016/S0341-8162(98)00056-3

Eppinga, M. B., de Ruiter, P. C., Wassen, M. J., & Rietkerk, M. (2009). Nutrients and hydrology indicate the driving mechanisms of peatland surface patterning. *The American Naturalist*, *173*, 803–818. https://doi.org/10.1086/598487

Eppinga, M. B., Rietkerk, M., Borren, W., Lapshina, E. D., Bleuten, W., & Wassen, M. J. (2008). Regular surface patterning of peatlands: Confronting theory with field data. *Ecosystems*, *11*, 520–536. https://doi.org/10.1007/s10021-008-9138-z

Fernandez-Oto, C., Escaff, D., & Cisternas, J. (2019). Spiral vegetation patterns in high-altitude wetlands. *Ecological Complexity*, *37*, 38–46. https://doi.org/10.1016/j.ecocom.2018.12.003

Fernandez-Oto, C., Tlidi, M., Escaff, D., & Clerc, M. G. (2014). Strong interaction between plants induces circular barren patches: Fairy circles. *Philosophical Transactions of the Royal Society A: Mathematical, Physical and Engineering Sciences*, *372*, 20140009. https://doi.org/10.1098/rsta.2014.0009

Getzin, S., Erickson, T. E., Yizhaq, H., Muñoz-Rojas, M., Huth, A., & Wiegand, K. (2020). Data from: Bridging ecology and physics: Australian fairy circles regenerate following model assumptions on ecohydrological feedbacks. *Zenodo*, https://doi.org/10.5281/zenodo.3979233

Getzin, S., Wiegand, K., & Schoening, I. (2012). Assessing biodiversity in forests using very high-resolution images and unmanned aerial vehicles. *Methods in Ecology and Evolution*, *3*, 397–404. https://doi.org/10.1111/j.2041-210X.2011.00158.x

Getzin, S., Wiegand, K., Wiegand, T., Yizhaq, H., von Hardenberg, J., & Meron, E. (2015a). Adopting a spatially explicit perspective to study the mysterious fairy circles of Namibia. *Ecography*, *38*, 1–11. https://doi.org/10.1111/ecog.00911

Getzin, S., Wiegand, K., Wiegand, T., Yizhaq, H., von Hardenberg, J., & Meron, E. (2015b). Clarifying misunderstandings regarding vegetation self-organization and spatial patterns of fairy circles in Namibia: A response to recent termite hypotheses. *Ecological Entomology*, *40*, 669–675. https://doi.org/10.1111/een.12267

Getzin, S., Yizhaq, H., Bell, B., Erickson, T. E., Postle, A. C., Katra, I., … Meron, E. (2016). Discovery of fairy circles in Australia supports self-organization theory. *Proceedings of the National Academy of Sciences of the United States of America*, *113*, 3551–3556. https://doi.org/10.1073/pnas.1522130113

Getzin, S., Yizhaq, H., Cramer, M. D., & Tschinkel, W. R. (2019). Contrasting global patterns of spatially periodic fairy circles and regular insect nests in drylands. *Journal of Geophysical Research: Biogeosciences*, *124*, 3327–3342. https://doi.org/10.1029/2019JG005393

Getzin, S., Yizhaq, H., Munoz-Rojas, M., Wiegand, K., & Erickson, T. E. (2019). A multi-scale study of Australian fairy circles using soil excavations and drone-based image analysis. *Ecosphere*, *10*, e02620. https://doi.org/10.1002/ecs2.2620

Gilad, E., von Hardenberg, J., Provenzale, A., Shachak, M., & Meron, E. (2004). Ecosystem engineers: From pattern formation to habitat creation. *Physical Review Letters*, *93*, 098105. https://doi.org/10.1103/PhysRevLett.93.098105

Grigg, A. M., Veneklaas, E. J., & Lambers, H. (2008). Water relations and mineral nutrition of *Triodia* grasses on desert dunes and interdunes. *Australian Journal of Botany*, *56*, 408–421. https://doi.org/10.1071/BT07156

Grimm, V., Revilla, E., Berger, U., Jeltsch, F., Mooij, W. M., Railsback, S. F., … DeAngelis, D. L. (2005). Pattern-oriented modelling of agent-based complex systems: Lessons from ecology. *Science*, *310*, 987–991. https://doi.org/10.1126/science.1116681

Haydon, D. T., Friar, J. K., & Pianka, E. R. (2000). Fire-driven dynamic mosaics in the Great Victoria Desert, Australia – II. A spatial and temporal landscape model. *Landscape Ecology*, *15*, 407–423. https://doi.org/10.1023/A:1008128214176

Hesselbarth, M. H. K., Sciaini, M., With, K. A., Wiegand, K., & Nowosad, J. (2019). landscapemetrics: An open-source R tool to calculate landscape metrics. *Ecography*, *42*, 1648–1657. https://doi.org/10.1111/ecog.04617

Holmgren, M., Scheffer, M., & Huston, M. A. (1997). The interplay of facilitation and competition in plant communities. *Ecology*, *78*, 1966–1975. https://doi.org/10.1890/0012-9658(1997)078[1966:TIOFAC]2.0.CO;2

Isbell, R. F. (2002). *The Australian soil classification* (Rev. ed.). Collingwood, Vic: CSIRO Publications.

Klausmeier, C. A. (1999). Regular and irregular patterns in semiarid vegetation. *Science*, *284*, 1826–1828. https://doi.org/10.1126/science.284.5421.1826

Kondo, S., & Miura, T. (2010). Reaction-diffusion model as a framework for understanding biological pattern formation. *Science*, *329*, 1616–1620. https://doi.org/10.1126/science.1179047

Lefever, R., & Lejeune, O. (1997). On the origin of tiger bush. *Bulletin of Mathematical Biology*, *59*, 263–294. https://doi.org/10.1007/BF02462004

Levin, N., Levental, S., & Morag, H. (2012). The effect of wildfires on vegetation cover and dune activity in Australia's desert dunes: A multisensor analysis. *International Journal of Wildland Fire*, *21*, 459–475. https://doi.org/10.1071/WF10150

McIntire, E. J. B., & Fajardo, A. (2009). Beyond description: The active and effective way to infer processes from spatial patterns. *Ecology*, *90*, 46–56. https://doi.org/10.1890/07-2096.1

Meron, E. (2012). Pattern-formation approach to modelling spatially extended ecosystems. *Ecological Modelling*, *234*, 70–82. https://doi.org/10.1016/j.ecolmodel.2011.05.035

Meron, E. (2015). *Nonlinear physics of ecosystems*. Boca Raton, FL: CRC Press. https://doi.org/10.1201/b18360

Meron, E. (2016). Pattern formation – A missing link in the study of ecosystem response to environmental changes. *Mathematical Biosciences*, *271*, 1–18. https://doi.org/10.1016/j.mbs.2015.10.015

Meron, E. (2018). From patterns to function in living systems: Dryland ecosystems as a case study. *Annual Review of Condensed Matter Physics*, *9*, 79–103. https://doi.org/10.1146/annurev-conmatphys-033117-053959

Meron, E., Bennett, J. J. R., Fernandez-Oto, C., Tzuk, O., Zelnik, Y. R., & Grafi, G. (2019). Continuum modeling of discrete plant communities: Why does it work and why is it advantageous? *Mathematics*, *7*, 987. https://doi.org/10.3390/math7100987

Meron, E., Gilad, E., von Hardenberg, J., Shachak, M., & Zarmi, Y. (2004). Vegetation patterns along a rainfall gradient. *Chaos, Solitons and Fractals*, *19*, 367–376. https://doi.org/10.1016/S0960-0779(03)00049-3

Muñoz-Rojas, M., Erickson, T. E., Martini, D., Dixon, K. W., & Merritt, D. J. (2016). Soil physicochemical and microbiological indicators of short, medium and long term post-fire recovery in semi-arid ecosystems. *Ecological Indicators*, *63*, 14–22. https://doi.org/10.1016/j.ecolind.2015.11.038

Newman, E. A., Kennedy, M. C., Falk, D. A., & McKenzie, D. (2019). Scaling and complexity in landscape ecology. *Frontiers in Ecology and Evolution*, *7*, 293. https://doi.org/10.3389/fevo.2019.00293

Palmer, J. (2016). Mysterious fairy circles now discovered in Australia's desert. *New Scientist*, *3065*.

Ravi, S., Wang, L., Kaseke, K. F., Buynevich, I. V., & Marais, E. (2017). Ecohydrological interactions within 'fairy circles' in the Namib Desert: Revisiting the self-organization hypothesis. *Journal of Geophysical Research: Biogeosciences*, *122*, 405–414. https://doi.org/10.1002/2016JG003604

Rietkerk, M., Boerlijst, M. C., van Langevelde, F., HilleRisLambers, R., van de Koppel, J., Kumar, L., … de Roos, A. M. (2002). Self-organization of vegetation in arid ecosystems. *The American Naturalist*, *160*, 524–530. https://doi.org/10.1086/342078

Rietkerk, M., Dekker, S. C., de Ruiter, P. C., & van de Koppel, J. (2004). Self-organized patchiness and catastrophic shifts in ecosystems. *Science*, *305*, 1926–1929. https://doi.org/10.1126/science.1101867

Rietkerk, M., & van de Koppel, J. (2008). Regular pattern formation in real ecosystems. *Trends in Ecology & Evolution*, *23*, 169–175. https://doi.org/10.1016/j.tree.2007.10.013

Ruiz-Reynés, D., Gomila, D., Sintes, T., Hernández-García, E., Marbà, N., & Duarte, C. M. (2017). Fairy circle landscapes under the sea. *Science Advances*, *3*, e1603262. https://doi.org/10.1126/sciadv.1603262

Saco, P. M., Willgoose, G. R., & Hancock, G. R. (2007). Eco-geomorphology of banded vegetation patterns in arid and semi-arid regions. *Hydrology and Earth System Sciences*, *11*, 1717–1730. https://doi.org/10.5194/hess-11-1717-2007

Saha, T., & Galic, M. (2018). Self-organization across scales: From molecules to organisms. *Philosophical Transactions of the Royal Society B: Biological Sciences*, *373*, 20170113. https://doi.org/10.1098/rstb.2017.0113

Sahagian, D. (2017). The magic of fairy circles: Built or created? *Journal of Geophysical Research: Biogeosciences*, *122*, 1294–1295. https://doi.org/10.1002/2017JG003855

Schurr, F. M., Bossdorf, O., Milton, S. J., & Schumacher, J. (2004). Spatial pattern formation in semi-arid shrubland: A priori predicted versus observed pattern characteristics. *Plant Ecology*, *173*, 271–282. https://doi.org/10.1023/B:VEGE.0000029335.13948.87

Sheffer, E., Yizhaq, H., Gilad, E., Shachak, M., & Meron, E. (2007). Why do plants in resource deprived environments form rings? *Ecological Complexity*, *4*, 192–200. https://doi.org/10.1016/j.ecocom.2007.06.008

Stoyan, D., & Stoyan, H. (1994). *Fractals, random shapes and point fields. Methods of geometrical statistics*. Chichester, UK: Wiley.

Tarnita, C. E., Bonachela, J. A., Sheffer, E., Guyton, J. A., Coverdale, T. C., Long, R. A., & Pringle, R. M. (2017). A theoretical foundation for multi-scale regular vegetation patterns. *Nature*, *541*, 398–401. https://doi.org/10.1038/nature20801

Tlidi, M., Lefever, R., & Vladimirov, A. (2008). On vegetation clustering, localized bare soil spots and fairy circles. *Lecture Notes in Physics*, *751*, 381–402. https://doi.org/10.1007/978-3-540-78217-9_15

Tschinkel, W. R. (2015). Experiments testing the causes of Namibian fairy circles. *PLoS ONE*, *10*, e0140099. https://doi.org/10.1371/journal.pone.0140099

Turing, A. M. (1952). The chemical basis of morphogenesis. *Philosophical Transactions of the Royal Society B: Biological Sciences*, *237*, 37–72. https://doi.org/10.1098/rstb.1952.0012

van Rooyen, M. W., Theron, G. K., van Rooyen, N., Jankowitz, W. J., & Matthews, W. S. (2004). Mysterious circles in the Namib Desert: Review of hypotheses on their origin. *Journal of Arid Environments*, *57*, 467–485. https://doi.org/10.1016/S0140-1963(03)00111-3

Vlieghe, K., & Picker, M. (2019). Do high soil temperatures on Namibian fairy circle discs explain the absence of vegetation? *PLoS ONE*, *14*, e0217153. https://doi.org/10.1371/journal.pone.0217153

von Hardenberg, J., Meron, E., Shachak, M., & Zarmi, Y. (2001). Diversity of vegetation patterns and desertification. *Physical Review Letters*, *87*, 198101. https://doi.org/10.1103/PhysRevLett.87.198101

Wiegand, K., Saltz, D., Ward, D., & Levin, S. A. (2008). The role of size inequality in self-thinning: A pattern-oriented simulation model for arid savannas. *Ecological Modelling*, *210*, 431–445. https://doi.org/10.1016/j.ecolmodel.2007.08.027

Wiegand, T., & Moloney, K. A. (2004). Rings, circles, and null-models for point pattern analysis in ecology. *Oikos*, *104*, 209–229. https://doi.org/10.1111/j.0030-1299.2004.12497.x

Worrall, G. A. (1959). The Butana grass patterns. *Journal of Soil Science*, *10*, 34–53. https://doi.org/10.1111/j.1365-2389.1959.tb00664.x

Yizhaq, H., & Bel, B. (2016). Effects of quenched disorder on critical transitions in pattern-forming systems. *New Journal of Physics*, *18*, 023004. https://doi.org/10.1088/1367-2630/18/2/023004

Yizhaq, H., Stavi, I., Swet, N., Zaady, E., & Katra, I. (2019). Vegetation ring formation by water overland flow in water-limited environments: Field measurements and mathematical modelling. *Ecohydrology*, *12*, e2135. https://doi.org/10.1002/eco.2135

Zelnik, Y. R., Meron, E., & Bel, G. (2015). Gradual regime shifts in fairy circles. *Proceedings of the National Academy of Sciences of the United States of America*, *112*, 12327–12331. https://doi.org/10.1073/pnas.1504289112

Zhu, Y., Getzin, S., Wiegand, T., Ren, H., & Ma, K. (2013). The relative importance of Janzen–Connell effects in influencing the spatial patterns at the Gutianshan Subtropical Forest. *PLoS ONE*, *8*, e74560. https://doi.org/10.1371/journal.pone.0074560

SUPPORTING INFORMATION

Additional supporting information may be found online in the Supporting Information section.

How to cite this article: Getzin S, Erickson TE, Yizhaq H, Muñoz-Rojas M, Huth A, Wiegand K. Bridging ecology and physics: Australian fairy circles regenerate following model assumptions on ecohydrological feedbacks. *J Ecol*. 2021;109:399–416. https://doi.org/10.1111/1365-2745.13493

Supporting Information for

Journal of Ecology

Bridging ecology and physics: Australian fairy circles regenerate following model assumptions on ecohydrological feedbacks

Stephan Getzin[1,2,†], Todd E. Erickson[3,4], Hezi Yizhaq[5], Miriam Muñoz-Rojas[3,4,6], Andreas Huth[2] & Kerstin Wiegand[1]

[1]Department of Ecosystem Modelling, University of Goettingen, Goettingen, Germany; [2]Department of Ecological Modelling, Helmholtz Centre for Environmental Research – UFZ, Leipzig, Germany; [3]School of Biological Sciences, The University of Western Australia, Crawley, WA, Australia; [4]Department of Biodiversity, Conservation and Attractions, Kings Park Science, Perth, WA, Australia; [5]Department of Solar Energy and Environmental Physics, Ben-Gurion University of the Negev, Sede Boqer, Israel and [6]School of Biological, Earth and Environmental Sciences, Centre for Ecosystem Science, UNSW Sydney, Sydney, NSW, Australia

[†]Corresponding author, email: stephan.getzin@uni-goettingen.de

TABLE S1 Summary of the used plots in this study and the applied measurements undertaken.

Plot name	Coordinates	Applied measurements
FC-L1	23°22'22"S, 119°54'17"E	NDVI-image of 100 m × 100 m plot: Berman test, spatial pattern analysis of high- and low-vitality grasses
FC-L2	23°21'33"S, 119°54'52"E	NDVI-image of 100 m × 100 m plot: Berman test, spatial pattern analysis of high- and low-vitality grasses; weather station data
FC-C2	23°22'50"S, 119°54'37"E	NDVI-image of 100 m × 100 m plot: Berman test, spatial pattern analysis of high- and low-vitality grasses; quadrat-based analysis of post-fire succession
FC-C5	23°21'40"S, 119°54'40"E	NDVI-image of 100 m × 100 m plot: Berman test, spatial pattern analysis of high- and low-vitality grasses
FC-1	23°26'52"S, 119°51'11"E	NDVI-image of 100 m × 100 m plot: Berman test, spatial pattern analysis of high- and low-vitality grasses
FC-F1	23°22'28"S, 119°54'28"E	Quadrat-based analysis of post-fire succession
FC-F3	23°22'19"S, 119°54'31"E	Quadrat-based analysis of post-fire succession

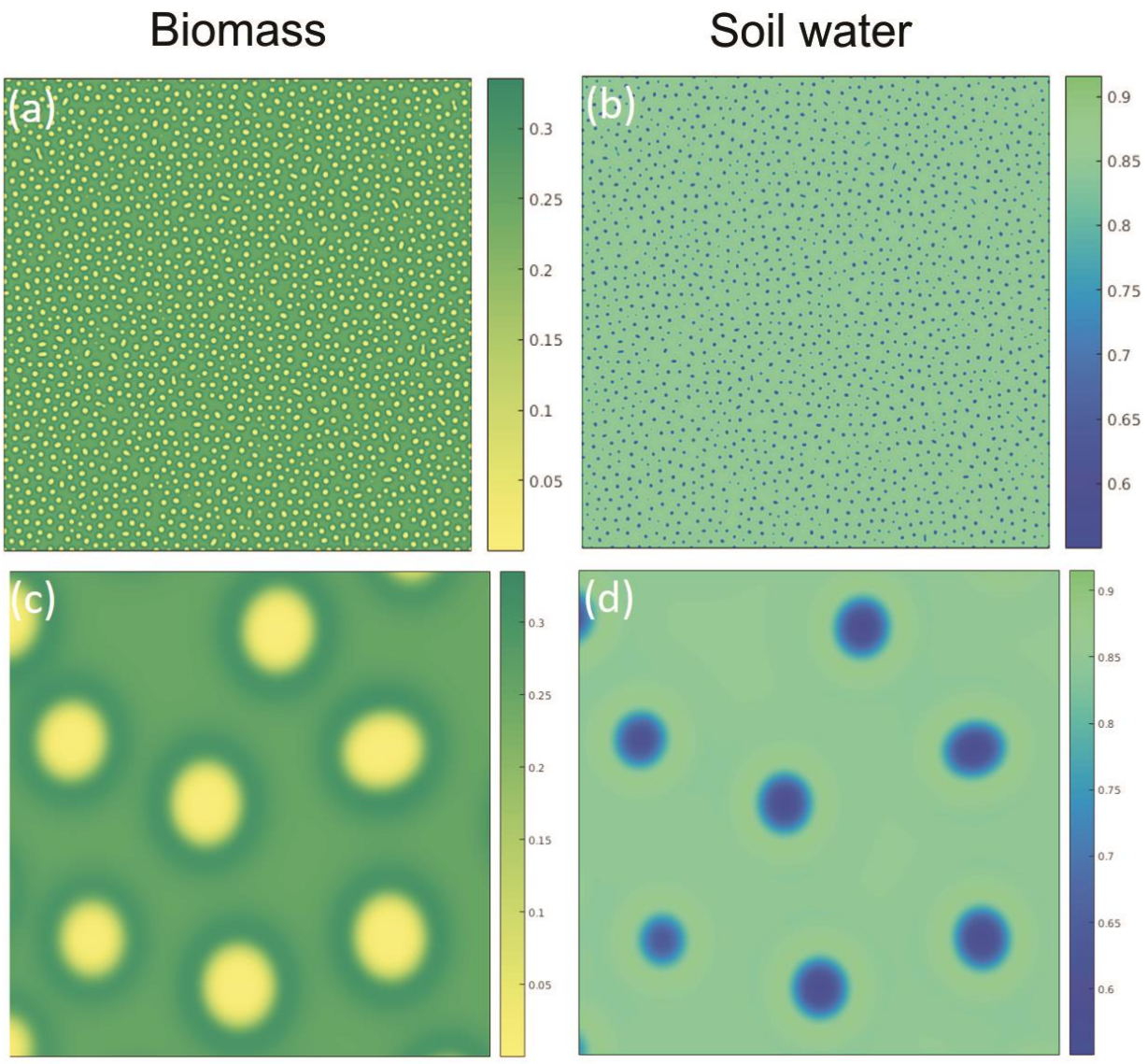

FIGURE S1 Modeled Australian fairy circles based on partial-differential equations and Turing instabilities. The spatially periodic pattern of FCs is shown as yellow gaps, whereas high biomass is indicated by green colour (a). The in-phase spatial profiles of biomass and soil water are indicated by corresponding blue colour, i.e. low soil-water content in the barren gap interior (b). The same properties are shown for zoomed images of biomass (c) and soil water (d) respectively. Note the ring of dark green colour around the FC periphery in (c). Details on the model can be found in Getzin et al. (2016).

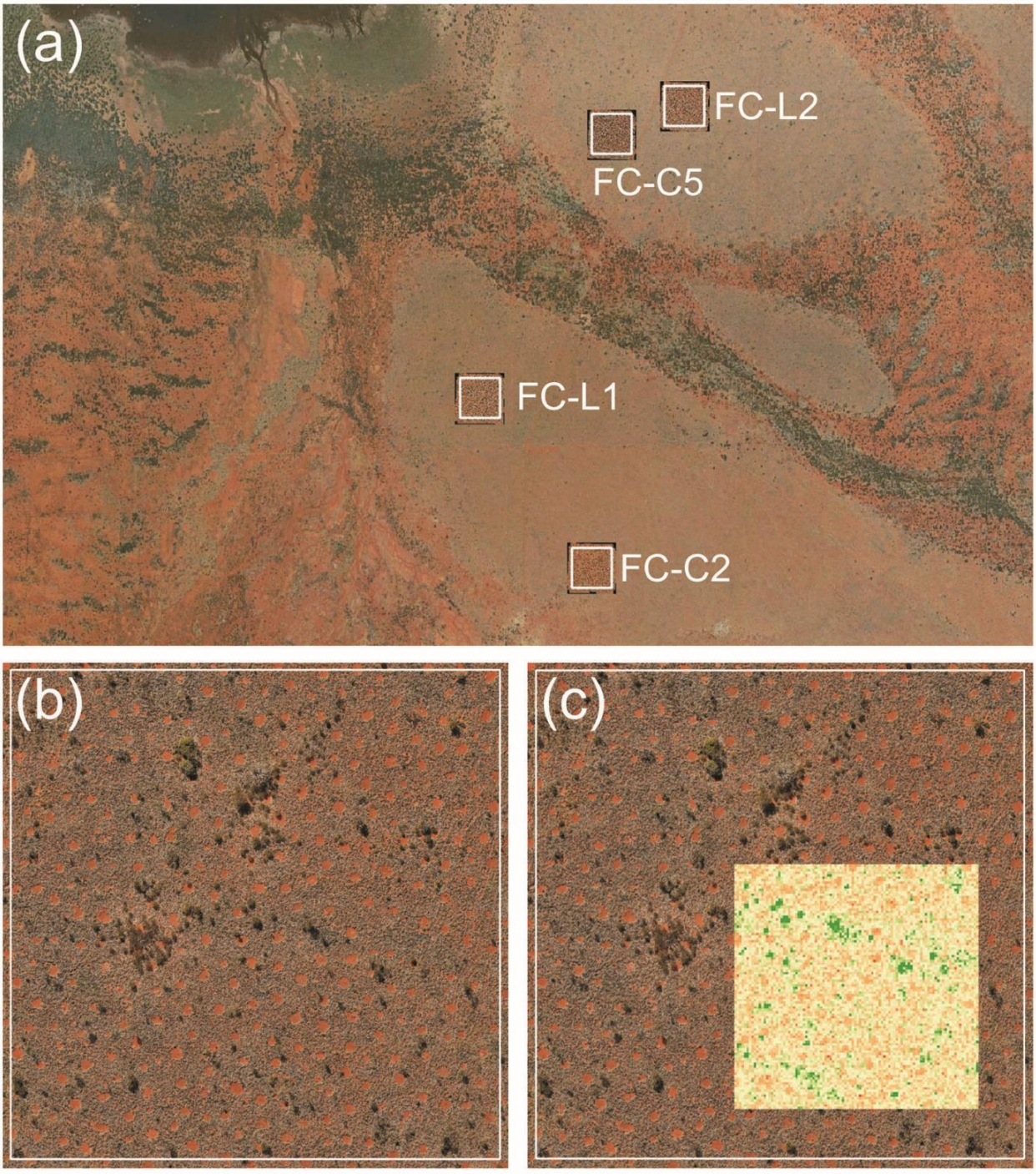

FIGURE S2 Locations of four 200 m × 200 m plots for which high-resolution RGB images were taken (a). Note the Ophthalmia Dam in the upper left corner. The fifth analyzed plot, FC-1, is not shown because it is located about 10 km to the south west. Example of the photographed 200 m × 200 m plot FC-C5 (b) and the selected 100 m × 100 m sub-window, used to analyze the NDVI with a grid resolution of 1 m × 1 m (c).

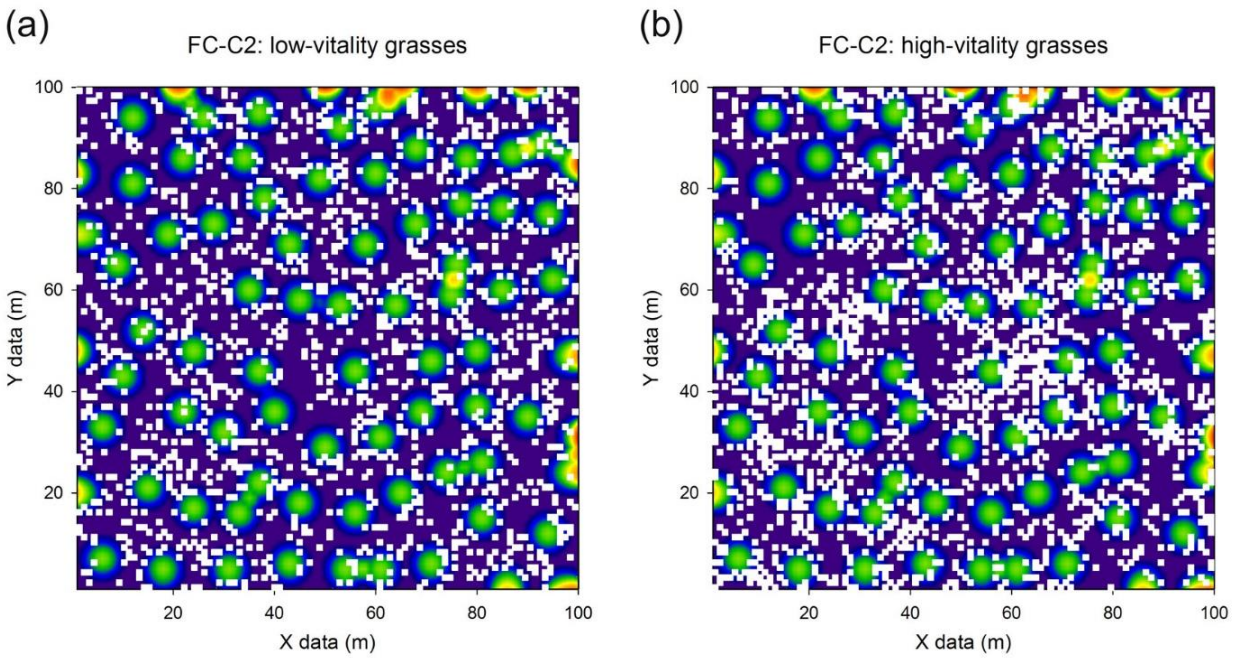

FIGURE S3 Example of the plot FC-C2 with the fairy circle locations converted into a kernel-smoothed covariate (Epanechnikov kernel with a radius of 5 m), which is a surrogate for extra water availability, provided by the FCs. The FCs are indicated by green colour. These same two spatial density maps were once overlayed with the position of the 1-m^2 NDVI cells representing low-vitality grasses (a) and once with the high-vitality grasses (b) to separately test for spatial association between grass vitality and the FCs, using the Berman test. These two types of grass cells were also analyzed for their spatial patterns using the null model of univariate random labelling, revealing that low-vitality grasses are typically segregated or randomly distributed while high-vitality grasses are clustered.

FIGURE S4 Locations of the quadrat-based mapping of post-fire recovery in March 2019 (a). The plots FC-F1, FC-C2, and FC-F3 burnt 3.5, 4.5, and > 15 years ago respectively. The quadrat placed in the matrix of the youngest plot FC-F1 (b,c). Examples of the quadrat placed in the matrix (d) and on the peripheral vegetation of a fairy circle (e) in the plot FC-C2. A burnt shrub and peripheral vegetation recovery in FC-C2 (f). Note how the peripheral grasses accumulate lignified plant material and litter around the circle's edge. Example of a fairy circle in the plot FC-F3 (g) and of a quadrat placed over the merging *Triodia* individuals at the gap's periphery (h). The grasses with their population-level behaviour act as "ecosystem engineers" to form a merged barrier, thereby maximizing their access to runoff from the gap (i). A horizontal perspective on the same group of grasses reveals a wall-like structure (j). Note the mechanical soil crusts in the foreground where water is trapped.

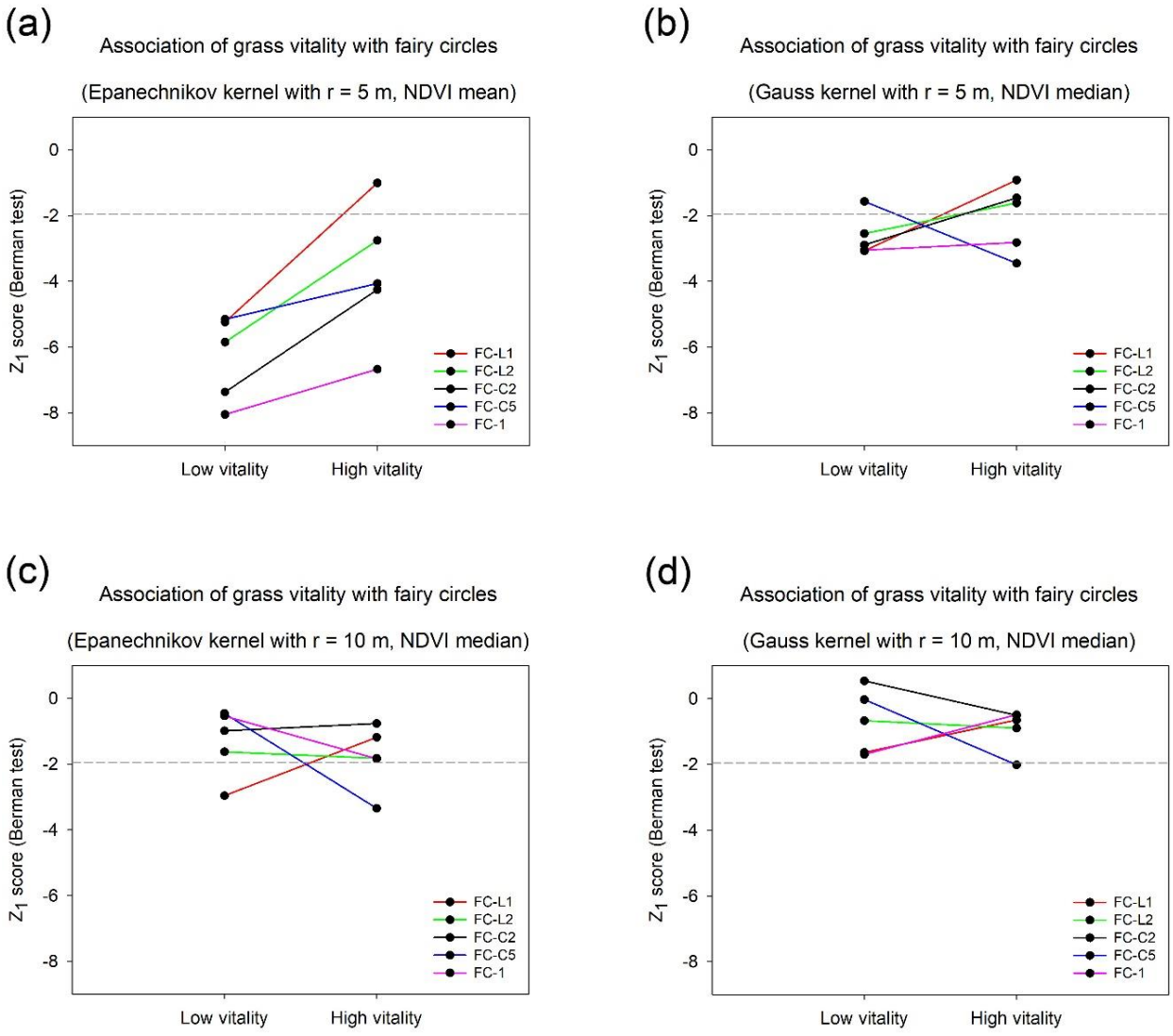

FIGURE S5 Testing the association of grass vitality with fairy circles for different kernel statistics. Using the mean (-0.10) instead of the median (-0.11) NDVI-value to differentiate between low-vitality (-0.15 to -0.10) and high-vitality (-0.09 to 0.10) grasses had no effect on the general outcome of the Berman test (a). As with using the median, high-vitality grasses were more strongly associated with FCs than low-vitality grasses and only the high-vitality grasses of the FC-L1 plot had a non-significant Z_1 score > -1.96, as indicated by the grey dashed line. By contrast, using a Gauss kernel and 5 m radius showed inconsistent results with four non-significant Z_1 scores and very low differences between low- and high-vitality grasses within plots (b). Additionally, an Epanechnikov kernel (c) with a radius of 10 m and a Gaussian kernel (d) with r = 10 m were also used to learn about the relationship of grass vitality and surrounding FCs. Somewhat expectedly, using kernels with a radius of 10 m resulted in blurry effects with a majority of grasses having non-significant Z_1 scores.

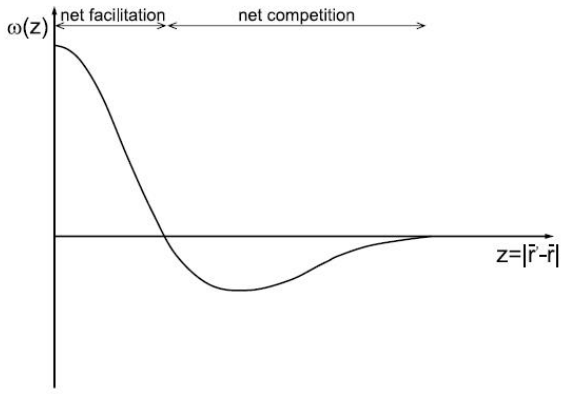

Figure 7. Typical kernel which exhibits local activation and long-range inhibition.

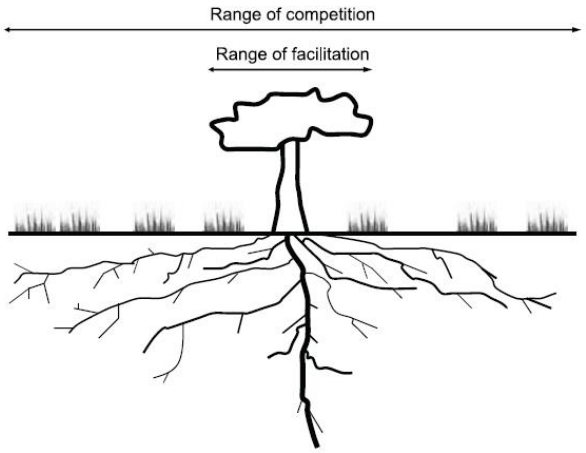

Figure 8. Visualization of the positive and negative interactions typical of a tree.

FIGURE S6 A short-distance positive feedback and a long-distance negative feedback, showing a higher magnitude of positive short-distance interaction than for negative long-distance interaction (left "Figure 7", after Borgogno et al., 2009). It is assumed that the feedback strength or magnitude of positive short-range interaction is larger because resource concentration and facilitation happens mainly around the smaller scale of plant crowns while competitive negative plant interactions happen more at the larger scale of plant roots, and ultimately the feedback strength vanishes with overall distances between plants (right "Figure 8", after Borgogno et al., 2009).